


Missing black holes in brightest cluster galaxies as evidence for the occurrence of superkicks in nature

Davide Gerosa¹ and Alberto Sesana²

¹*Department of Applied Mathematics and Theoretical Physics, Centre for Mathematical Sciences, University of Cambridge, Wilberforce Road, Cambridge CB3 0WA, UK*

²*Max-Planck-Institut für Gravitationsphysik, Albert Einstein Institut, Am Mühlenberg 1, D-14476 Golm, Germany*

Accepted 2014 September 30. Received 2014 September 2; in original form 2014 May 6

ABSTRACT

We investigate the consequences of superkicks on the population of supermassive black holes (SMBHs) in the Universe residing in brightest cluster galaxies (BCGs). There is strong observational evidence that BCGs grew prominently at late times (up to a factor 2–4 in mass from $z = 1$), mainly through mergers with satellite galaxies from the cluster, and they are known to host the most massive SMBHs ever observed. Those SMBHs are also expected to grow hierarchically, experiencing a series of mergers with other SMBHs brought in by merging satellites. Because of the net linear momentum taken away from the asymmetric gravitational wave emission, the remnant SMBH experiences a kick in the opposite direction. Kicks may be as large as 5000 km s^{-1} (‘superkicks’), pushing the SMBHs out in the cluster outskirts for a time comparable to galaxy-evolution time-scales. We predict, under a number of plausible assumptions, that superkicks can efficiently eject SMBHs from BCGs, bringing their occupation fraction down to a likely range $0.9 < f < 0.99$ in the local Universe. Future thirty-metre-class telescopes like ELT and TMT will be capable of measuring SMBHs in hundreds of BCGs up to $z = 0.2$, testing the occurrence of superkicks in nature and the strong-gravity regime of SMBH mergers.

Key words: Black hole physics – gravitation – gravitational waves – galaxies: evolution – galaxies: interactions.

1 INTRODUCTION

The centres of galaxy clusters host the most massive galaxies in the Universe, generally known as brightest cluster galaxies (BCGs). Their luminosity can easily exceed $10^{12} L_{\odot}$ and, consequently, their estimated masses can be up to few times $10^{12} M_{\odot}$. They also host the biggest supermassive black holes (SMBHs) known in the Universe, with masses in the range 10^9 – $10^{10} M_{\odot}$ (McConnell et al. 2012), tipping the observed SMBH–host relations at the high-mass end (McConnell & Ma 2013).

In the context of the Λ cold dark matter (Λ CDM) cosmological paradigm, large dark matter (DM) haloes in the Universe build up hierarchically (White & Rees 1978), driving the assembly of galactic structures. Galaxy formation kicks off at high redshifts, as gas starts to cool at the centres of DM haloes. Following the halo hierarchy, small protogalaxies merge with each other forming larger ones. This process continues until the present time, resulting in the formation of massive galaxies we see today. Within this framework also SMBHs grow hierarchically, experiencing a sequence of accretion events and merging with other SMBHs following galaxy

mergers (Begelman, Blandford & Rees 1980; Volonteri, Haardt & Madau 2003).

One interesting astrophysical consequence of SMBH binary mergers is the gravitational recoil. Emission of asymmetric gravitational waves (GWs) in the late inspiral and final coalescence takes away net linear momentum from the binary system, and the remnant SMBH is consequently kicked in the opposite direction. With the advent of numerical relativity (Pretorius 2005; Baker et al. 2006; Campanelli et al. 2006), it is now possible to simulate SMBH mergers in full general relativity and assess the magnitude of these kicks. Surprisingly, configurations have been found in which the final kick can reach magnitudes up to $\sim 5000 \text{ km s}^{-1}$ (Campanelli et al. 2007; González et al. 2007a; Lousto & Zlochower 2011)¹ opening the possibility of SMBH ejection even from the deepest potential wells created by the most massive galaxies (Merritt et al. 2004;

¹ Technically, Campanelli et al. (2007); González et al. (2007a) found recoils up to $\sim 4000 \text{ km s}^{-1}$ for systems with spins lying in the binary orbital plane, which they referred to as ‘superkicks’. ‘Hangup kicks’ up to $\sim 5000 \text{ km s}^{-1}$ were found by Lousto & Zlochower (2011) in a different configuration, in which the spins are inclined with respect to the orbital plane of the binary. For simplicity, we will generally refer to high-velocity recoils as ‘superkicks’ throughout the paper.

*E-mail: d.gerosa@damtp.cam.ac.uk

Schnittman & Buonanno 2007). Observationally, few candidate recoiling SMBHs have been recently identified as off-centre AGNs (Civano et al. 2010, 2012; Koss et al. 2014), and an excellent review of the spatial and kinematical observational signatures of these peculiar systems can be found in Komossa (2012). A direct consequence of high-velocity kicks is that the SMBH occupation fraction may be altered (Schnittman 2007; Volonteri, Haardt & Gültekin 2008; Volonteri, Gültekin & Dotti 2010), providing an indirect way to test the strong-gravity physics behind GW kicks. In this paper, we explore this possibility by investigating the consequences of gravitational recoils on to SMBH masses and the occupation fraction in BCGs.

Although kicks will naturally eject SMBHs more easily from lighter galaxies (as extensively investigated by Volonteri et al. 2010), there are at least three good reasons for considering this possibility in BCGs. First, BCGs show the strongest mass evolution from $z \approx 1.5$ up to now. In general, both detailed numerical simulations of galaxy formation (De Lucia & Blaizot 2007; Oser et al. 2010; Lackner et al. 2012) and observations of BCGs at different z (Trujillo, Ferreras & de La Rosa 2011; Lidman et al. 2012, 2013) show an average mass doubling from $z = 1$ to the present time. Though it is difficult to assess observationally what is the cause of this mass growth, it appears in simulations to be driven primarily by galaxy mergers (Lotz et al. 2011; Laporte et al. 2013). This is also consistent with close galaxy pair counts at $z < 1$ (Bell et al. 2006; Bundy et al. 2009; de Ravel et al. 2009; Robaina et al. 2010; López-Sanjuan et al. 2012; Xu et al. 2012), which imply a prominent merger activity for these systems. In contrast with all other types of galaxies, very massive ellipticals (and BCGs in particular) are expected to have undergone several mergers in the last 10 Gyr, some of them ‘major’ (i.e. with satellite to primary galaxy mass ratio $M_2/M_1 > 1/4$). It is therefore possible that they also experienced a few SMBH binary coalescences, with consequent gravitational recoils. Secondly, SMBHs of mass $> 10^9 M_\odot$ in the relatively low-density environment of BCG nuclei have the largest impact on the dynamics of the surrounding stars (McConnell et al. 2012). The influence radius of the SMBH can be up to few hundred parsecs, making them ideal targets for direct dynamical measurements of SMBH masses. With angular resolutions of ≈ 0.1 arcsec, it is today possible to confidently measure SMBH masses in BCGs up to $z \approx 0.03$. A factor of 10 improvement in the instrumentation, expected with the Thirty Metre Telescope (TMT) and the European Extremely Large Telescope (ELT), will dramatically increase this range. As an example, Do et al. (2014) estimated that 50 masses of SMBHs residing in BCGs up to $z = 0.05$ can be measured with a relatively cheap programme of 14 observing nights on the TMT. Moreover, they show that the TMT potential will be much greater than that, making mass measurement possible in hundreds of BCGs up to $z \approx 0.2$. Conversely, in Milky Way-type galaxies with SMBH sphere of influence of the order of few parsecs, even with ELT precision dynamical measurements will be restricted to our local neighbourhood ($D < 30$ Mpc, $z < 0.01$). Lastly, according to our galaxy formation knowledge, the SMBH occupation fraction f (i.e. the fraction of galaxies hosting a SMBH) is an increasing function of the galaxy mass. Although already at dwarf galaxy scales f might be around unity (Bellovary et al. 2011), observations of galaxies in Virgo galaxies show a sudden drop in the X-ray activity at stellar masses around $10^{10} M_\odot$ (Miller et al. 2012). Although this cannot be taken as evidence of lack of nuclear SMBHs, there is no observational confirmation of a large f for galaxies on those small scales.

Some tentative candidates of SMBH ejections from BCGs have already been identified: the BCG in the A2261 cluster shows an

exceptionally large core of 3.2 kpc consistent with the absence of a scouring SMBH (Postman et al. 2012); the small $1.2 \times 10^{11} M_\odot$ lenticular galaxy NCG 1277 in the Perseus cluster hosts an exceptionally heavy SMBH of $1.7 \times 10^{10} M_\odot$ (van den Bosch et al. 2012) which may have grown in the close BCG NCG 1275, ejected by a superkick and finally captured by NCG 1277 (Shields & Bonning 2013).

Summarizing, BCGs, being the most massive galaxies in the Universe, (i) are expected to have $f = 1$; (ii) have possibly experienced multiple mergers at low redshift; (iii) are the easiest targets for nuclear SMBH mass measurements. These facts make them ideal targets for observing the effects of extreme recoils: any observational confirmation of a missing nuclear SMBH would provide strong evidence for the occurrence of superkicks.

The paper is organized as follows. Section 2 presents the ingredients of our models: (i) SMBH merger fitting formulas; (ii) galaxy density profiles; (iii) prescriptions for the SMBH return time-scales and (iv) the merger events; and (v) finally our evolutionary procedure. We highlight our results in Section 3 and present our conclusions in Section 4. Throughout this paper, we use a Λ CDM cosmological model with $\Omega_M = 0.27$, $\Omega_\Lambda = 0.73$ and $H_0 = 100 h \text{ km s}^{-1} \text{ Mpc}^{-1} = 70 \text{ km s}^{-1} \text{ Mpc}^{-1}$.

2 BCG MERGER MODELLING

A thoughtful modelling of the recoil effect on the SMBH occupation fraction in BCGs requires putting together in a coherent framework four main ingredients:

- (i) the recoil magnitude as a function of the SMBH binary parameters (binary mass ratio, magnitude and orientation of the individual SMBH spins);
- (ii) the gravitational potential in which the recoiled SMBH evolves;
- (iii) the return time-scale for SMBHs suffering kicks below the escape velocity of their hosts;
- (iv) the number of mergers experienced by BCGs as a function of z and of the galaxy mass ratio.

We will describe each item separately in the following subsections, providing in Section 2.5 a description of the ‘coherent framework’ that brings them together; we point the readers not interested in all the mathematical details of our model directly to that section.

2.1 Black hole final mass, spin and kick velocity

We start with modelling the properties of the remnant SMBH as a function of the properties of the progenitor merging holes. We use a standard notation in which m_1 and m_2 denote the individual masses of the merging SMBHs (with $m_1 > m_2$), $M = m_1 + m_2$ is the total mass, $q = m_2/m_1 \leq 1$ is the mass ratio and $\eta = m_1 m_2 / M^2$ is the symmetric mass ratio. The SMBH spin vectors are (with $i = 1, 2$)

$$\mathbf{S}_i = \chi_i \frac{G m_i^2}{c} \hat{\mathbf{S}}_i, \quad (1)$$

where $0 \leq \chi_i \leq 1$ is the dimensionless spin parameter and hats denote unit vectors. We describe the directions of the spins $\hat{\mathbf{S}}_i$ with three angles θ_1 , θ_2 and $\Delta\Phi$ defined to be (cf. fig. 1 in Gerosa et al. 2014)

$$\begin{aligned} \cos \theta_1 &= \hat{\mathbf{S}}_1 \cdot \hat{\mathbf{L}}, & \cos \theta_2 &= \hat{\mathbf{S}}_2 \cdot \hat{\mathbf{L}}, \\ \cos \Delta\Phi &= \frac{\hat{\mathbf{S}}_1 \times \hat{\mathbf{L}}}{|\hat{\mathbf{S}}_1 \times \hat{\mathbf{L}}|} \cdot \frac{\hat{\mathbf{S}}_2 \times \hat{\mathbf{L}}}{|\hat{\mathbf{S}}_2 \times \hat{\mathbf{L}}|}, \end{aligned} \quad (2)$$

where $\hat{\mathbf{L}}$ is the (instantaneous) direction of the orbital angular momentum of the binary. It is also useful to define the following quantities.

$$\mathbf{\Delta} = \frac{q\chi_2\hat{\mathbf{S}}_2 - \chi_1\hat{\mathbf{S}}_1}{1+q}, \quad \tilde{\chi} = \frac{q^2\chi_2\hat{\mathbf{S}}_2 + \chi_1\hat{\mathbf{S}}_1}{(1+q)^2}, \quad (3)$$

and to introduce the subscripts \parallel and \perp for vector components along/perpendicular to the orbital angular momentum of the binary:

$$\tilde{\chi}_{\parallel} = \tilde{\chi} \cdot \hat{\mathbf{L}}, \quad \tilde{\chi}_{\perp} = |\tilde{\chi} \times \hat{\mathbf{L}}|, \quad \Delta_{\parallel} = \mathbf{\Delta} \cdot \hat{\mathbf{L}}, \quad \Delta_{\perp} = |\mathbf{\Delta} \times \hat{\mathbf{L}}|.$$

The energy radiated during the inspiral and merger phase E_{rad} reduces the post-merger mass to $M_f = M - E_{\text{rad}}c^{-2}$. The dependence of E_{rad} on the initial parameters (namely the masses and the spins) can be derived analytically in the test-particle limit $q \rightarrow 0$ (Kesden 2008), while the comparable-mass regime $q \simeq 1$ can only be estimated using full numerical relativity simulations (Berti et al. 2007; Tichy & Marronetti 2008; Lousto et al. 2010). Here, we use the expression recently provided by Barausse, Morozova & Rezzolla (2012), in which the two regimes are interpolated

$$\frac{E_{\text{rad}}}{M} = 1 - \frac{M_f}{M} = \eta \left[1 - E'_{\text{ISCO}} \right] + 4\eta^2 \left[4p_0 + 16p_1\tilde{\chi}_{\parallel} (\tilde{\chi}_{\parallel} + 1) + E'_{\text{ISCO}} - 1 \right], \quad (4)$$

where $c^2 E'_{\text{ISCO}}$ is the energy per unit mass at the innermost stable circular orbit (ISCO) in the test-particle limit generalized to inclined orbits and evaluated at the effective spin $\tilde{\chi}$ (Bardeen 1973):

$$E'_{\text{ISCO}} = \sqrt{1 - \frac{2}{3r'_{\text{ISCO}}}}, \quad (5)$$

$$r'_{\text{ISCO}} = 3 + Z_2 - \text{sign}(\tilde{\chi}_{\parallel})\sqrt{(3 - Z_1)(3 + Z_1 + 2Z_2)}, \quad (6)$$

$$Z_1 = 1 + (1 - \tilde{\chi}_{\parallel}^2)^{1/3} \left[(1 + \tilde{\chi}_{\parallel})^{1/3} + (1 - \tilde{\chi}_{\parallel})^{1/3} \right], \quad (7)$$

$$Z_2 = \sqrt{3\tilde{\chi}_{\parallel}^2 + Z_1^2}. \quad (8)$$

The parameters p_0 and p_1 in equation (4) were fitted by Barausse et al. (2012) using the numerical relativity data published at the time (see references therein): they report $p_0 = 0.04827$ and $p_1 = 0.01707$.

The final spin magnitude χ_f has been predicted either by calibrating fitting formulas with numerical relativity simulations (Rezzolla et al. 2008; Tichy & Marronetti 2008; Barausse & Rezzolla 2009; Lousto et al. 2010), or by extrapolating test-particle results (Buonanno, Kidder & Lehner 2008; Kesden 2008). Here, we use the expression developed by Barausse & Rezzolla (2009), which has been shown to reproduce the available numerical relativity data with 8 per cent precision in χ_f for every value of q :

$$\chi_f = \left| \tilde{\chi} + \frac{q}{(1+q)^2} \ell \hat{\mathbf{L}} \right|, \quad (9)$$

$$\ell = 2\sqrt{3} + t_2\eta + t_3\eta^2 + s_4 \frac{(1+q)^4}{(1+q^2)^2} \tilde{\chi}^2 + (s_5\eta + t_0 + 2) \frac{(1+q)^2}{1+q^2} \tilde{\chi}_{\parallel}. \quad (10)$$

The remaining free parameters are fitted to numerical relativity simulations (see Barausse & Rezzolla 2009 for details): $t_0 = -2.8904$, $t_2 = -3.51712$, $t_3 = 2.5763$, $s_4 = -0.1229$ and $s_5 = 0.4537$. We assume $\chi_f = 1$ whenever the fitting formula (9) predicts higher unphysical values.

GW recoils generally arise from asymmetries in the merging binary that could be either in the masses or in the spins. Fitting

formulas for the recoil velocity \mathbf{v}_k are typically broken down into a mass asymmetry term v_m , and two spin asymmetry terms $v_{s\parallel}$ and $v_{s\perp}$ (Campanelli et al. 2007):

$$\mathbf{v}_k = v_m \mathbf{e}_{\perp 1} + v_{s\perp} (\cos \xi \mathbf{e}_{\perp 1} + \sin \xi \mathbf{e}_{\perp 2}) + v_{s\parallel} \hat{\mathbf{L}}, \quad (11)$$

where $\mathbf{e}_{\perp 1}$, $\mathbf{e}_{\perp 2}$ are two orthogonal unit vectors in the orbital plane and ξ is the angle between the mass term and the orbital-plane spin term. Expressions for v_m , $v_{s\parallel}$ and $v_{s\perp}$ are available as fitting formulas to the numerical simulations. In this work, we implement the following expressions:

$$v_m = A\eta^2 \frac{1-q}{1+q} (1 + B\eta), \quad (12)$$

$$v_{s\perp} = H\eta^2 \Delta_{\parallel}, \quad (13)$$

$$v_{s\parallel} = 16\eta^2 [\Delta_{\perp} (V_{11} + 2V_A \tilde{\chi}_{\parallel} + 4V_B \tilde{\chi}_{\parallel}^2 + 8V_C \tilde{\chi}_{\parallel}^3) + \tilde{\chi}_{\perp} \Delta_{\parallel} (2C_2 + 4C_3 \tilde{\chi}_{\parallel})] \cos \Theta. \quad (14)$$

The term proportional to V_{11} in equation (14) arises from the superkick formula (Campanelli et al. 2007; González et al. 2007b), the terms in $V_{A,B,C}$ have been called ‘hangup-kick’ effect (Lousto & Zlochower 2011), while the ones proportional to $C_{2,3}$ model the newly discovered ‘cross-kick’ effect (Lousto & Zlochower 2013). The parameters in the equations above are currently estimated to be: $A = 1.2 \times 10^4 \text{ km s}^{-1}$, $B = -0.93$ (González et al. 2007a), $H = 6.9 \times 10^3 \text{ km s}^{-1}$ (Lousto & Zlochower 2008), $V_{11} = 3677.76 \text{ km s}^{-1}$, $V_A = 2481.21 \text{ km s}^{-1}$, $V_B = 1792.45 \text{ km s}^{-1}$, $V_C = 1506.52 \text{ km s}^{-1}$ (Lousto et al. 2012), $C_2 = 1140 \text{ km s}^{-1}$, $C_3 = 2481 \text{ km s}^{-1}$ (Lousto & Zlochower 2013), $\xi = 145^\circ$ (Lousto & Zlochower 2008). The value of the angle Θ actually depends on the initial separation of the binary in the numerical simulations: as in previous studies (Berti, Kesden & Sperhake 2012; Lousto et al. 2012), we deal with this dependence by sampling over a uniform distribution in Θ .

Since the spin angles θ_1 , θ_2 and $\Delta\Phi$ evolve during the inspiral, the recoil fitting formula provided above can only be applied close to merger, at separations $a \sim 10M$ where numerical relativity simulations typically start.² Kesden, Sperhake & Berti (2010b) pointed out that substantial recoil suppression/enhancement could occur due to spin-orbit resonances (Schnittman 2004) in the post-Newtonian (PN) regime of the inspiral. Spin-orbit resonances mostly affect binaries with asymmetric spin directions at large separation ($\theta_1 \neq \theta_2$), while symmetric configurations ($\theta_1 \simeq \theta_2$) are generally unaffected (Gerosa et al. 2013). Both effects are generally present for isotropic distributions of the spin angles that are therefore maintained qualitatively isotropic by the PN evolution (Bogdanović, Reynolds & Miller 2007; Kesden, Sperhake & Berti 2010a). Resonant effects are therefore strongly dependent on early-time alignment processes, such as those arising from accretion-disc interactions (Perego et al. 2009; Dotti et al. 2010; Lodato & Gerosa 2013; Miller & Krolik 2013).

In the present astrophysical application to BCG galaxies, we assume isotropic distributions of both the spin vectors, taking the spin angles uniformly distributed in $\cos \theta_1$, $\cos \theta_2$ and $\Delta\Phi$. This is a delicate point because the misalignment distribution (also needed to

² The effect of PN resonances is critical to compute the kick velocity, but not so critical in the case of the final mass (equation 4) and the final spin (equation 9): see Barausse & Rezzolla (2009) for a discussion of this point.

properly initialize the late-time PN inspiral) has a strong impact on the recoil velocities. Although spin alignment is expected to occur when a SMBH binary is surrounded by a cold massive circumbinary disc, the relative cold gas content of galaxies is a decreasing function of their mass (Catinella et al. 2010) and BCGs are extremely gas-poor systems. Fresh cold gas can be naturally brought in by the merging satellite; however, most of the companions of massive elliptical galaxies in observed galaxy pairs are red (up to about 70 per cent; López-Sanjuan et al. 2012), making dry mergers the more common mass growth channel for BCGs. None the less, a fraction of mergers can still result in significant accretion on to the central SMBH; in fact, BCGs are known to power luminous radio jets (Best et al. 2007) creating X-ray cavities in a number of clusters (Hlavacek-Larrondo et al. 2013; Russell et al. 2013). However, as a result of the ‘anti-hierarchical’ behaviour of AGNs, only about one in a thousand of the SMBHs with $M > 3 \times 10^8 M_\odot$ is accreting at more than 1 per cent of the Eddington rate at low redshift (Heckman et al. 2004). This is despite the fact that very massive galaxies experience (as we will see below) a prominent merger activity at $z < 1$. Assuming one merger per BCG since $z = 1$, the numbers above imply that BCGs are, on average, accreting at about 1 per cent of the Eddington rate for $\sim 10^7$ yr, resulting in a mass growth < 1 per cent. This is generally insufficient to align the spins of a putative SMBH binary even if the gas is accreted by a coherent circumbinary pool as envisaged by Dotti et al. (2010). Moreover, accretion might occur in a series of subsequent episodes with incoherent angular momenta orientations (King & Pringle 2006; Sesana et al. 2014), and disc spin alignment might be less effective than generally assumed in simple α -disc models (Lodato & Gerosa 2013). Therefore, disc-driven alignment processes should be less important for the systems relevant to our investigation, and random spin orientation is a sensible working hypothesis for the majority of them. In this case, the kick distribution is only weakly modified by the PN inspiral (cf. Berti et al. 2012, their fig. 2) and can therefore be neglected. We checked and confirm this conclusion using the numerical PN code presented by Gerosa et al. (2013). This is particularly important because following the full PN evolution is computationally expensive; bypassing this stage allows us to simulate a larger number of galaxies, thus reducing the statistical error on the final occupation fractions. For reasonably large samples (~ 1000 BCGs), uncertainties in the occupation fraction are still dominated by Poisson counting errors, rather than the PN influence on the kicks.

2.2 BCG mass-density and potential profile

BCGs sit at the centre of their host cluster. The relevant potential is therefore given by the spheroidal component of the BCG plus the whole cluster DM halo.

A simple analytic model to describe the spheroidal component is given by the Hernquist mass-density profile (Hernquist 1990; Tremaine et al. 1994; see Laporte et al. 2013 for a specific application to BCGs):

$$\rho_{\text{BCG}}(r) = \frac{M_{\text{BCG}}}{2\pi} \frac{r_{\text{H}}}{r} \frac{1}{(r + r_{\text{H}})^3}, \quad (15)$$

where M_{BCG} is the mass of the spheroid and r_{H} is a scale radius. The scale radius r_{H} can be related to the typical cusp radius r_{γ} observed in the luminosity profiles of elliptical galaxies (Carollo et al. 1997; Lauer et al. 2007). We match cusp-radius measurements from Lauer et al. (2007) and galaxy-mass measurements from McConnell & Ma

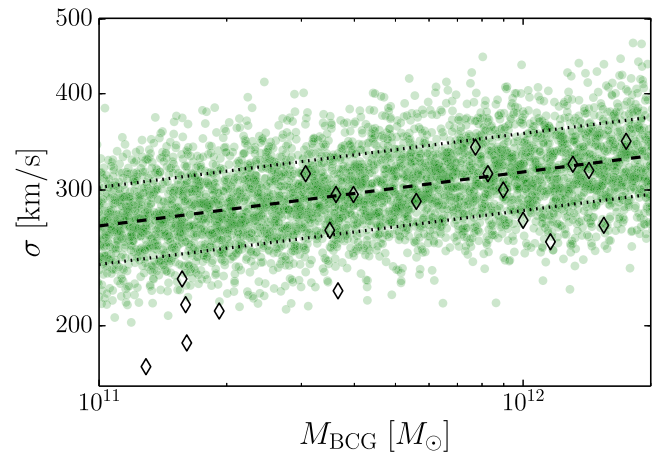


Figure 1. BCG kinematical properties, modelled using the Hernquist profile. The velocity dispersion values predicted from our model are compared with the sample of observations reported by McConnell & Ma (2013, black diamonds). Green circle points are computed sampling equation (16) with a Gaussian error of 0.1 dex and then considering $\sigma \approx 0.3\sqrt{GM_{\text{BCG}}/r_{\text{H}}}$ (Hernquist 1990); black dashed and dotted lines show the average and the 1σ interval of the same distribution.

(2013), obtaining a final sample of 14 BCGs. We fit these values using a log–log relation, obtaining

$$\log\left(\frac{r_{\gamma}}{\text{pc}}\right) = -7.73 + 0.857 \log\left(\frac{M_{\text{BCG}}}{M_{\odot}}\right), \quad (16)$$

with dispersion of 0.1 dex. The central densities of elliptical cores typically lie in the range 10^3 – $10^4 M_{\odot} \text{pc}^{-3}$ (see e.g. Terzić & Graham 2005); these values are reproduced by scaling the cusp radius by an order of magnitude, i.e. taking $r_{\text{H}} = 10r_{\gamma}$. This choice gives acceptable results in terms of the kinematical properties of BCGs, especially at typical BCG masses $\sim 10^{12} M_{\odot}$: Fig. 1 shows the velocity dispersion of the BCG $\sigma \approx 0.3\sqrt{GM_{\text{BCG}}/r_{\text{H}}}$ (Hernquist 1990) compared³ to the measurements in the sample of large elliptical galaxies collected by McConnell & Ma (2013).

Self-consistent (and therefore more realistic) models have also been developed to describe photometric and kinematical data in elliptical galaxies (see e.g. Bertin 2000) but we opted for the Hernquist profile because it reproduces the kinematical properties quite well despite its analytical simplicity. We model the cluster DM halo with a Navarro–Frenk–White (NFW) profile (Navarro, Frenk & White 1996, 1997), which has been found to be in good agreement with galaxy cluster data (van der Marel et al. 2000). The NFW mass-density profile is

$$\rho_{\text{DM}}(r) = \frac{c^3 g_c \Delta_v(z)}{3} \rho_c(z) \frac{1}{(cr/r_v)(1 + cr/r_v)^2}, \quad (17)$$

where r_v is the virial radius; $\Delta_v(z)$ is the virial overdensity (see below); c is a concentration parameter; the function g_c is given by

$$g_c = \frac{1}{\ln(1 + c) - c/(1 + c)}; \quad (18)$$

³ Since the baryonic structure is much more concentrated than the DM halo (i.e. $r_{\text{H}} \ll r_v$), considering the stellar component only is sufficient in a comparison with stellar-velocity data. The definition of σ used by McConnell & Ma (2013) involves measurements of velocity dispersion and radial velocity averaged up to some effective radius (their equation 1). We compare their estimates with values of σ evaluated close to r_{H} , where the Hernquist profile is expected to give the largest contribution to their averaged estimations.

and $\rho_c(z)$ is the critical density of the Universe at the redshift under consideration,

$$\rho_c(z) = \frac{3H^2(z)}{8\pi G}, \quad (19)$$

where

$$H(z) = H_0 \sqrt{(1+z)^3 \Omega_M + \Omega_\Lambda}. \quad (20)$$

The virial radius r_v is defined as the distance from the centre of the halo within which the mean density is $\Delta_v(z)\rho_c(z)$. The halo mass M_{DM} is then simply defined to be the DM mass within r_v :

$$M_{\text{DM}} = \frac{4}{3}\pi r_v^3 \Delta_v(z)\rho_c(z). \quad (21)$$

Under the assumption that the cluster has just virialized,⁴ calculations of spherical top-hat perturbations (Peebles 1980) yield $\Delta_v = 18\pi^2 \simeq 178$, but the actual value depends on the cosmological model through (Lacey & Cole 1993; Bryan & Norman 1998; Klypin, Trujillo-Gomez & Primack 2011)

$$\Delta_v(z) = 18\pi^2 - 82\Omega_\Lambda(z) - 39\Omega_\Lambda^2(z), \quad (22)$$

where

$$\Omega_M(z) = \frac{(1+z)^3 \Omega_M}{(1+z)^3 \Omega_M + \Omega_\Lambda}, \quad \Omega_\Lambda(z) = 1 - \Omega_M(z). \quad (23)$$

The virial radius as a function of the halo mass reads

$$r_v = \left(\frac{M_{\text{DM}}}{10^{14} M_\odot} \right)^{1/3} \left(\frac{\Omega_M}{\Omega_M(z)} \frac{\Delta_v(z)}{18\pi^2} \right)^{-1/3} \frac{1 \text{ Mpc}}{1+z}. \quad (24)$$

In the regime considered here ($z < 1$), the virial overdensity Δ_v is roughly $0.7 \times 18\pi^2 \simeq 124$ with a rather weak dependence on z ; typical sizes of DM haloes with the same mass may differ by a factor ~ 1.5 if placed at different redshifts.

Stott et al. (2012) relate the BCG visible mass to the halo mass measured at r_{500} , defined to be the radius at which the mean density is 500 times the critical density of the *present* Universe:

$$M_{500} = \frac{4}{3}\pi r_{500}^3 \rho_c(z=0) \times 500. \quad (25)$$

Their observational relation reads (Stott et al. 2012)

$$\log \left(\frac{M_{500}}{10^{14} M_\odot} \right) = -14.29 + 1.28 \log \left(\frac{M_{\text{BCG}}}{M_\odot} \right), \quad (26)$$

with dispersion $\sigma \approx 0.3$ dex. The concentration parameter c is related to the halo mass and in general depends on the redshift and the underlying cosmological model (Neto et al. 2007; Macciò, Dutton & van den Bosch 2008; Ludlow et al. 2014). Those dependences are, however, rather weak in the BCG range ($M_{200} \sim 10^{13-16} M_\odot$), in which theoretical predictions by different authors tend to agree (see fig. 10 in Ludlow et al. 2014). Here, we implement the relation reported by Neto et al. (2007):

$$\log c = 5.26 - 0.1 \log \left(\frac{M_{200}}{10^{14} M_\odot} h^{-1} \right), \quad (27)$$

with a dispersion of 0.05 dex. In analogy with equation (26), M_{200} is defined to be the mass of the halo inside a radius r_{200} at which

⁴ For simplicity, we do not truncate the NFW halo at the virial radius, which is expected under such virialization assumption (e.g. Peacock 2003; Barausse 2012). Our predictions of the final occupation fractions are independent of these assumptions: SMBHs kicked at $r_{\text{max}} > r_v \sim \text{few Mpc}$ in general do not find their way back to the galactic centre within a Hubble time.

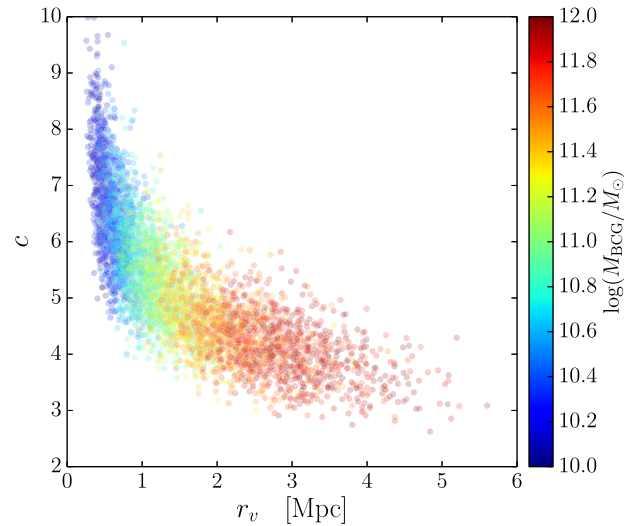


Figure 2. Observationally based relation between the halo virial radius r_v and the concentration parameter c . Fitting formulas provided by Stott et al. (2012) and Neto et al. (2007) are solved using the iterative procedure described in the main text. M_{BCG} is reported on the colour scale. Massive galaxies (lighter points on the right) correspond to larger haloes and to lower values of c ; on the other hand, lighter BCGs (darker points on the left) are hosted in smaller haloes and present a wider range of concentrations up to $c \simeq 10$. This figure is obtained with a uniform distribution in $\log M_{\text{BCG}}/M_\odot \in [10, 12]$ at $z = 0$.

the mean density is 200 times the critical density:

$$M_{200} = \frac{4}{3}\pi r_{200}^3 \rho_c(z=0) \times 200. \quad (28)$$

The value of M_{500} and M_{200} can also be obtained by integrating $\rho_{\text{DM}}(r)$ from equation (17). This gives the following constraints on r_{200} , r_{500} and r_v :

$$\frac{500}{\Delta_v} \frac{H_0^2}{H^2(z)} = g_c \left(\frac{r_v}{r_{500}} \right)^3 \left[\ln \left(1 + \frac{cr_{500}}{r_v} \right) - \frac{cr_{500}/r_v}{1 + cr_{500}/r_v} \right]; \quad (29)$$

$$\frac{200}{\Delta_v} \frac{H_0^2}{H^2(z)} = g_c \left(\frac{r_v}{r_{200}} \right)^3 \left[\ln \left(1 + \frac{cr_{200}}{r_v} \right) - \frac{cr_{200}/r_v}{1 + cr_{200}/r_v} \right]. \quad (30)$$

We implement an iterative procedure to find r_v and c simultaneously; results are presented in Fig. 2.

For each BCG stellar mass, M_{BCG} , we compute M_{500} through equation (26) assuming a Gaussian error of 0.3 dex, and then r_{500} using equation (25). Given the initial guess $c = 5$, the constraint (29) is used to obtain numerically r_v . Equation (30) is then solved to find r_{200} , and M_{200} is obtained using equation (28). An updated value of c can now be computed through the observational relation (27). The whole procedure is then iterated. When convergence is reached,⁵ we add a Gaussian error of 0.05 dex to the final value of c . Once r_v and c are obtained, the halo mass, M_{DM} , is given by equation (21). As a consistency test, the BCG/DM-halo relation is shown in Fig. 3, where our Monte Carlo sample is contrasted to observational data from Lidman et al. (2012).

⁵ Convergence down to $|\Delta c| < 10^{-6}$ is typically obtained after five iterations.

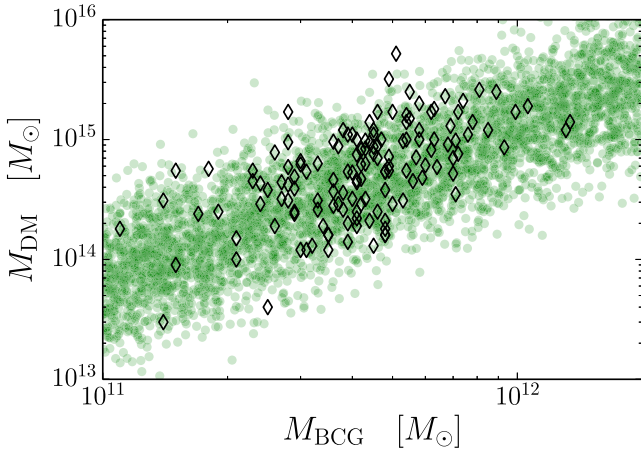


Figure 3. Relation between M_{BCG} and M_{DM} as implemented in our model. Our Monte Carlo realization (green circles) is statistically consistent with the observational catalogue of 160 BCGs collected by Lidman et al. (2012, black diamonds). This figure is obtained with uniform distributions in $\log M_{\text{BCG}}/M_{\odot} \in [11, 12.3]$ and $z \in [0, 1.5]$, which are the same ranges covered by the data sample in Lidman et al. (2012).

To summarize: we model the BCG mass density from equations (15) and (17) as $\rho = \rho_{\text{BCG}} + \rho_{\text{DM}}$, while the associated gravitational potential is given by $\Phi = \Phi_{\text{BCG}} + \Phi_{\text{DM}}$, with

$$\Phi_{\text{BCG}}(r) = -\frac{GM_{\text{BCG}}}{r + r_{\text{H}}}, \quad (31)$$

and

$$\Phi_{\text{DM}}(r) = -g_{\text{c}} \frac{GM_{\text{DM}}}{r_{\text{v}}} \frac{\ln(1 + cr/r_{\text{v}})}{r/r_{\text{v}}}. \quad (32)$$

2.3 Recoiled SMBH return time-scales

Following the binary merger, the remnant SMBH recoils because of asymmetrical GW emission which may result in its ejection from the BCG core. The recoiling SMBH transfers its orbital energy into random motions of the surrounding stars through collisions, and may sink back to the galactic centre. Here, we develop two physical models to predict the return time-scale of this process.

The remnant SMBH is initially kicked out on a radial orbit. Detailed N -body simulations of the process have been performed by Gualandris & Merritt (2008), which detect strong damping during each passage of the SMBH through the galactic core. It is therefore critical to know whether the recoiling SMBH orbit crosses the galactic core, since damping happens mainly in those quick passages. Repeated core passages cannot be prevented in a spherically symmetric potential. However, post-merger galactic potentials are expected to be triaxial (Khan, Just & Merritt 2011; Preto et al. 2011): the SMBH orbit will not in general remain exactly radial and in particular the core may not be crossed (Vicari, Capuzzo-Dolcetta & Merritt 2007). Moreover, especially for extreme kicks, the SMBH can travel further than a Mpc from the BCG core. At this point, its trajectory is likely to be perturbed by the clumpy potential of other galaxies and DM subhaloes within the main cluster halo, and return to the BCG core is unlikely. Missing the core would result in a much longer inspiral time-scale because only low-density regions contribute to the frictional force. This difference is critical to our purposes, particularly if this time-scale gets comparable with the time-scale between two galactic mergers: less efficient sinking may result in ‘empty’ galactic centres when the next satellite galaxy

merges into the BCG. The full complexity of the problem cannot be solved within our spherically symmetric model; therefore, we developed two extreme approaches bracketing the uncertainties related to the dynamics describe above.

(i) In the first model, we assume that the SMBH orbit is ‘quasi-circular’ and we compute the sinking time-scale using Chandrasekhar’s (1943) dynamical friction (DF). This is meant to be the extreme case for a strongly perturbed potential for which the SMBH never crosses the galactic core.

(ii) In the second scenario, we consider repeated SMBH-core bounces by fitting the N -body simulations reported by Gualandris & Merritt (2008). This model is appropriate for BCG and cluster potentials which exhibit small deviations from spherical symmetry.

2.3.1 Dynamical friction model

Let us consider a SMBH with mass M_{BH} kicked with velocity v_{k} from the galactic centre ($r = 0$). The SMBH will be ejected from the galactic halo if v_{k} exceeds the escape velocity of the system:

$$v_{\text{esc}} = \sqrt{2G \left(\frac{M_{\text{BCG}}}{r_{\text{H}}} + c g_{\text{c}} \frac{M_{\text{DM}}}{r_{\text{v}}} \right)}. \quad (33)$$

If $v_{\text{k}} < v_{\text{esc}}$, the SMBH will stop at a distance r_{max} from the centre. Gualandris & Merritt (2008) showed that the maximum displacement r_{max} can be estimated simply through energy conservation neglecting star friction (see their fig. 2):

$$\frac{1}{2}v_{\text{k}}^2 + \phi(0) = \phi(r_{\text{max}}). \quad (34)$$

The initial displacement is reached in a time which is typically 100 times smaller than the sinking time-scale (Gualandris & Merritt 2008) and will be therefore neglected. Here, we estimate the time needed to sink back to $r = 0$ integrating the DF equation on quasi-circular orbits. The frictional force exerted on to the black hole is given by (e.g. Binney & Tremaine 1987)

$$F(r) = \frac{4\pi G^2 M_{\text{BH}}^2 \rho(r) \xi(r) \ln \Lambda}{v_{\text{c}}^2(r)}, \quad (35)$$

where $v_{\text{c}}(r) = \sqrt{r d\phi/dr}$ is the circular velocity, $\ln \Lambda$ is the Coulomb logarithm and the factor $\xi(r)$ depends on the stellar velocity distribution. We take $\ln \Lambda = 2.5$, as observed by Gualandris & Merritt (2008) in the very first phase of their simulated orbits (see also Escala et al. 2004). We assume the velocity distribution to be locally Maxwellian, with velocity dispersion $\sigma(r)$. Although not exact, the Maxwellian distribution is approached as a consequence of collisionless relaxation processes (Lynden-Bell 1967). Under this assumption, the ξ factor in equation (35) reads (Binney & Tremaine 1987)

$$\xi(r) = \text{erf} \left[\frac{v_{\text{c}}(r)}{\sqrt{2}\sigma(r)} \right] - \sqrt{\frac{2}{\pi}} \frac{v_{\text{c}}(r)}{\sigma(r)} \exp \left[-\frac{v_{\text{c}}^2(r)}{2\sigma^2(r)} \right]. \quad (36)$$

The velocity dispersion $\sigma(r)$ is computed from our galactic potential using the expression provided by Binney (1980) when isotropy is assumed. The frictional force $F(r)$ is tangential and directed opposite to the SMBH velocity. The SMBH angular momentum $L(r) = M_{\text{BH}}rv_{\text{c}}(r)$ is lost at the rate $dL(r)/dt = -rF(r)$ by Newton’s third law, causing the SMBH to slowly inspiral while remaining on a quasi-circular orbit. The DF time-scale, over which the SMBH sinks back to the galactic centre $r = 0$ from its initial position r_{max} ,

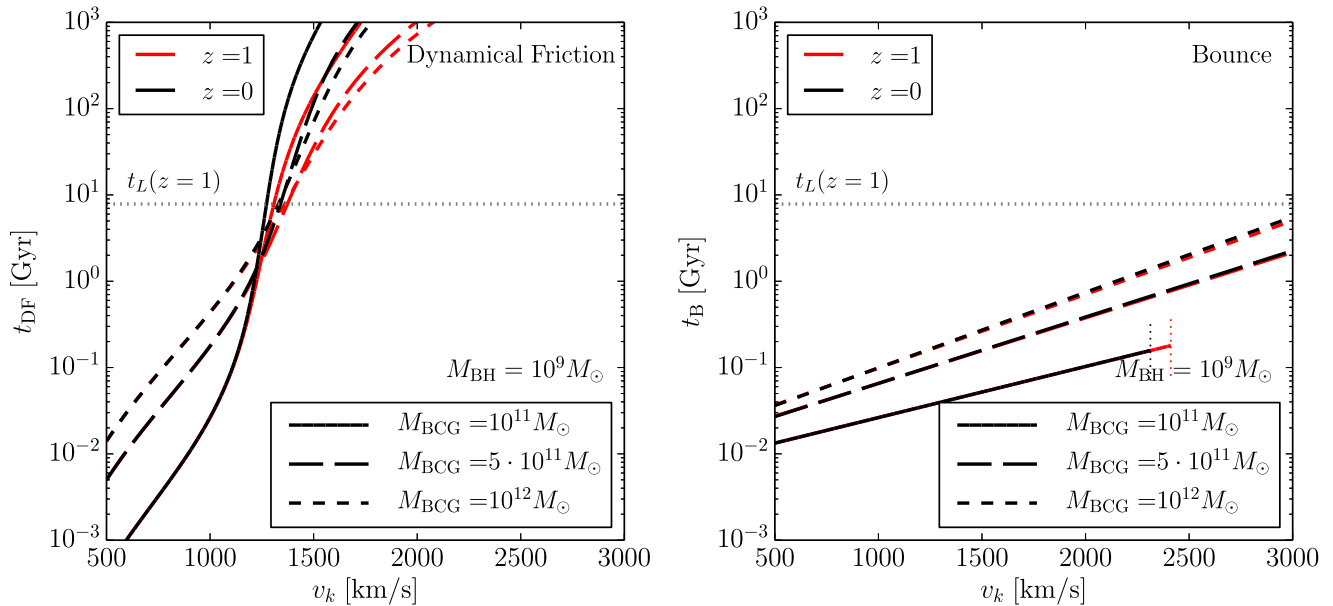


Figure 4. SMBH return time-scales, in both the DF (left) and the bounce model (right), as a function of the kick velocity v_k . We consider recoiling SMBHs with $M_{\text{BH}} = 10^9 M_{\odot}$ and BCGs with stellar mass $M_{\text{BCG}} = 10^{11} M_{\odot}$ (solid), $5 \cdot 10^{11} M_{\odot}$ (long-dashed) and $10^{12} M_{\odot}$ (short-dashed). The remaining galaxy parameters (such as r_{H} , M_{DM} , r_v and c) are estimated using the prescriptions presented in Section 2.2. To facilitate comparisons, here we set variances in equations (16), (26) and (27) to zero. In order to bracket the effects of cosmological evolution we carry out the analysis at both $z = 0$ (darker, black lines) and $z = 1$ (lighter, red lines). Black holes are effectively ejected from the BCGs when the sinking time-scale (either t_{DF} or t_{B}) gets larger than the lookback time at the merger redshift, which in turn is always smaller than the one computed at $z = 1$ (~ 7.8 Gyr, shown with a dotted horizontal line). Dotted vertical lines in the right panel are placed at the escape velocity v_{esc} , at which equation (40) must be truncated.

is thus given by⁶

$$t_{\text{DF}} = - \int_{r_{\text{max}}}^0 \frac{dL(r)}{dr} \frac{1}{r F(r)} dr. \quad (37)$$

DF time-scales for typical systems are reported in Fig. 4 (left-hand panel) as a function of the kick velocity v_k . A recoiling SMBH is strictly ejected only if $v_k > v_{\text{esc}}$, which is unlikely since we are considering the whole cluster potential for which v_{esc} may be as large as $\sim 6000 \text{ km s}^{-1}$ for the typical values $M_{\text{BCG}} = 10^{12} M_{\odot}$ and $M_{\text{BH}} = 10^9 M_{\odot}$. However, SMBHs are effectively ejected if their return time-scales are larger than the lookback time at the merger redshift z_m (e.g. Peebles 1993):

$$t_L(z_m) = \int_0^{z_m} \frac{dz}{(1+z)H(z)}, \quad (38)$$

which corresponds to the time the Universe needs to evolve from z_m to now. In this case, the SMBH remains outside the BCG, wandering in the intracluster medium. Our systems are evolved from $z = 1$ to 0, which sets a (conservative) effective escape condition $t_{\text{DF}} > t_L(z = 1)$ for which SMBHs will never come back to the BCG centre. As shown in the left-hand panel of Fig. 4, this condition is

⁶ Because of the intrinsic divergence in the density profile (equations 15–17), this integral cannot be computed up to $r = 0$: hereafter, we implement a lower threshold at $10^{-3} r_{\text{H}} \sim 1 \text{ pc}$. We also neglect the dependence on the redshift while computing the integral (equation 37). In both models, the sinking times are computed fixing the redshift at his initial value (i.e. when the kick is imparted to the SMBH). As shown in Fig. 4, differences between time-scales computed at different redshifts are negligible in the interesting region $t_{\text{DF}} < t_L(z = 1)$.

fulfilled for achievable kicks $v_k \sim 1500 \text{ km s}^{-1}$, opening the possibility of several (effective) ejections from typical BCGs. When this occurs, the distance between the SMBH and the galaxy centre (offset) can be estimated by numerically inverting equation (37). At $z = 0$, the SMBH needs the additional time $t_{\text{DF}} - t_L(z_m)$ to sink to the centre. The offset $r_{z=0}$ is given by the displacement resulting in such time,⁷ i.e.

$$t_{\text{DF}} - t_L(z_m) = - \int_{r_{z=0}}^0 \frac{dL(r)}{dr} \frac{1}{r F(r)} dr. \quad (39)$$

2.3.2 Bounce model

To describe recoiling SMBHs on radial orbit, we rely on the N -body simulations performed by Gualandris & Merritt (2008). They study the motion of a SMBH recoiling from the centre of an initially spherically symmetric galaxy. The SMBH motion can be divided into three distinct stages: (i) first, a short DF phase damps the radial oscillations as predicted by Chandrasekhar’s (1943) formula with $2 \lesssim \ln \Lambda \lesssim 3$; (ii) once the amplitude of the motion is smaller than the core radius, the SMBH and the galactic core exhibit oscillations about their common centre of mass; (iii) finally, the SMBH and the core reach thermal equilibrium when the SMBH kinetic energy equals the mean kinetic energy of the stars in the core. Orbital energy dissipation occurs mostly during core-SMBH encounters. Here, we are interested in estimating the time-scale t_{B} , given by the sum of the first and the second phase.

The duration of the first two phases is listed in Gualandris & Merritt (2008) for 18 simulations in total, six in each of their three

⁷ In both scenarios, offsets are computed with the galaxy properties at $z = 0$.

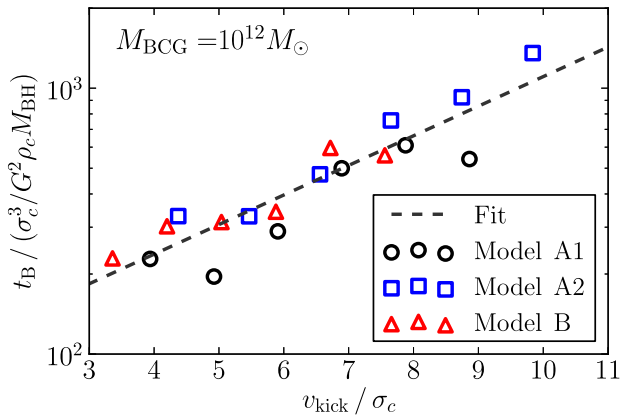


Figure 5. Fitting curve employed to compute the return time-scale in the bounce model t_B as a function of the kick velocity v_{kick} . Markers show predictions computed by Gualandris & Merritt (2008) in each of their models, namely *A1*, *A2* and *B*. Once reduced to dimensionless quantities with the expected scaling, all three models appear to lie on the same lin–log relation, which however must be truncated at the escape velocity v_{esc} . The dimensionless scaled points and the fitting curve (dashed black line) depend only weakly on the galaxy mass M_{BCG} . This figure is produced with $M = 10^{12} M_{\odot}$; the resulting fitting coefficients are $a = 0.26$ and $b = 4.44$.

different models. As suggested by the authors themselves (their equation 18), the second-phase times originally reported must be corrected, since the number of N -body particles used is smaller than the actual number of stars in a galaxy. They implement the galaxy profile first proposed by Terzić & Graham (2005) to describe binary-depleted galactic cores which present a well-defined profile transition at the core radius r_c . Oscillations damp only during passages through the galaxy core, whose properties are expected to strongly influence the damping time. For a given M_{BCG} , we first compute the SMBH mass M_{BH} , the velocity dispersion σ_c and the mass density ρ_c at r_c for each of their three models using the Terzić & Graham (2005) density profile. Even if DF cannot fully describe such core-passage dynamics, the return time appears to satisfy the same scaling relation as if DF would be fully responsible for the sinking process (Gualandris & Merritt 2008). We therefore scale the simulated kick velocities with σ_c and the reported return time-scales t_B with $\sigma_c^3 / G^2 \rho_c M_{\text{BH}}$.

Once reduced to a dimensionless problem, we fit their 18 simulated time-scales with the ansatz

$$t_B = \frac{\sigma_c^3}{G^2 \rho_c M_{\text{BH}}} \exp\left(a \frac{v}{\sigma_c} + b\right), \quad (40)$$

truncated at the escape velocity v_{esc} . Here a and b are best-fitting coefficients. They only depend (weakly) on the galactic mass M_{BCG} which enters in the correction factor to t_B due to the limited number of N -body particles. Fig. 5 shows the results of our fit for a fiducial mass $M_{\text{BCG}} = 10^{12} M_{\odot}$. The dimensionless fit can be reported into physical units by computing σ_c and ρ_c for our galactic profiles (Hernquist+NFW) at a fiducial core radius

$$\log\left(\frac{r_c}{\text{pc}}\right) \simeq 1.1 + 0.09 \log\left(\frac{r_H}{\text{pc}}\right), \quad (41)$$

as obtained by matching the mass dependences in equation (16) with the analogous estimate for the core radius used by Gualandris & Merritt (2008). Results of our procedure are reported in the right-hand panel of Fig. 4. This second model predicts longer inspiral time-scales for kicks smaller than $\sim 1000 \text{ km s}^{-1}$; while large kicks make SMBHs returning very quickly ($\sim 100 \text{ Myr}$) to their galactic

centres. If the SMBH does not escape from the cluster ($v < v_{\text{esc}}$), there will always be a first core passage causing enough dissipation to trigger more and more passages leading to a quick comeback.

The SMBH offset at $z = 0$ can be computed by iterating the fit procedure describe above. We numerically look for the hypothetical kick velocity \tilde{v}_k which would result in a return time equal to $t_B - t_L(z_m)$, i.e. the time left to the SMBH at $z = 0$ to finally reach the galactic centre. Assuming the SMBH motion to be approximately oscillatory, we compute the amplitude of the oscillations $\tilde{r}_{z=0}$ from energy conservation (cf. equation 34) and we finally estimate the offset to be $r_{z=0} = \tilde{r}_{z=0} \sin \varphi$, with φ uniformly distributed in $[0, \pi]$.

2.4 BCG merger rates

In the last few years, strong observational evidence for a prominent growth of BCGs from $z = 1$ came about. Among other studies, Trujillo et al. (2011) observe that early-type galaxies grew by a factor 5–10 in size and 2–4 in mass since $z = 1$, and Lidman et al. (2012) find that BCGs grow in mass by a factor of ≈ 2 in the redshift range 0.9–0.2 (see also Burke & Collins 2013 and Ascaso et al. 2014). BCG mass growth is naturally explained by frequent mergers in the hierarchical build-up scenario, and several dedicated simulations and theoretical studies find that major and minor mergers can account for it (De Lucia & Blaizot 2007; Oser et al. 2010; Lackner et al. 2012; Laporte et al. 2013). However, there are claims that size growth cannot be ascribed to mergers, and might be related to the redshift evolution of the properties of the underlying DM haloes (Posti et al. 2014; Sonnenfeld, Nipoti & Treu 2014). In general, the merger-driven mass-growth scenario is consistent with observations of close galaxy pairs (Bundy et al. 2009; de Ravel et al. 2009; Liu et al. 2009; Robaina et al. 2010; López-Sanjuan et al. 2012; Xu et al. 2012), and both observations and simulations point towards high merger rates for early-type galaxies (Hopkins et al. 2010; Lotz et al. 2011), that can be up to 0.4 Gyr^{-1} at $z \sim 1$ for BCGs (Lidman et al. 2013).

Here, we exploit the observationally based approach put forward by Sesana (2013). We are not interested in a global galaxy-merger rate, but rather in the distribution of mergers experienced by the typical BCG. Building on the same formalism as in Sesana (2013), the galaxy merger rate per unit mass ratio⁸ and redshift experienced by a galaxy of a given mass can be written as

$$\left. \frac{d^2 N}{dz dQ} \right|_M = \left. \frac{df}{dQ} \right|_{M,z} \frac{1}{\tau(z, M, Q)} \frac{dt_L}{dz}. \quad (42)$$

Here, $df/dQ|_{M,z}$ is the differential fraction of galaxies with mass M at redshift z paired with a secondary galaxy having a mass ratio in the range $[Q, Q + \delta Q]$; $\tau(z, M, Q)$ is the typical merger time-scale for a galaxy pair with a given M and Q at a given z ; and dt_L/dz is the integrand in equation (38). df/dQ can be directly measured from observations, whereas τ can be inferred by detailed numerical simulations of galaxy mergers. The number of mergers experienced from $z = 1$ to 0 by a galaxy starting with mass $M_{\text{BCG}} = M_{z=1}$ at $z = 1$ can be therefore written as

$$N(M_{z=1}) = \int_1^0 dz \int_{Q_{\min}}^1 dQ \int dM \left. \frac{d^2 N}{dz dQ} \right|_M \delta[M - M(z)], \quad (43)$$

where the integral is consistently evaluated at the redshift-evolving galaxy mass $M(z)$ through the Dirac delta function.

⁸ We indicate galaxy mass ratios with Q , to differentiate with black holes mass ratios q .

To estimate the mass growth of BCGs, we consider the fraction f of galaxies with a companion in the range $Q_{\min} = 0.25 < Q < 1$, which corresponds to the standard definition of major mergers. f is estimated in several observational studies, and it is generally fitted with a function of redshift of the form

$$f = a(1+z)^b. \quad (44)$$

The parameters a and b are, in general, function of the primary galaxy mass. Since we are concerned with BCGs, we consider fits to equation (44) corresponding to primaries with mass $M > 10^{11} M_{\odot}$. We construct three models, to which we will refer as ‘Optimistic’, ‘Fiducial’ and ‘Pessimistic’. In the ‘Fiducial’ model we take the best fit to the observations of Bundy et al. (2009), yielding $a = 0.035$, $b = 1.3$. Those data are consistent with a larger fraction described by $a = 0.07$, $b = 0.7$, which we take as ‘Optimistic’ model. López-Sanjuan et al. (2012) find a smaller pair fraction with a stronger redshift dependence, corresponding to $a = 0.02$, $b = 1.8$, which we take as ‘Pessimistic’ model. Pairs are then distributed across the allowed mass ratio range according to $df/dQ|_{M,z} \propto Q^{-1}$ (López-Sanjuan et al. 2011). López-Sanjuan et al. (2012) additionally provide the pair fraction in the range $0.1 < Q < 0.25$, corresponding to minor mergers. This is found to be $f \approx 0.06$ independent on redshift. We add those to the ‘Pessimistic’ model to construct the ‘Pessimistic-Minor’ model, which we use to assess the impact of minor mergers on our findings.

The function τ is then specified by using the formula given by Kitzbichler & White (2008, their equation 10) to get⁹

$$\tau = 1.32 \text{ Gyr} \left(\frac{M_*}{4 \times 10^{10} h^{-1} M_{\odot}} \right)^{-0.3} \left(1 + \frac{z}{8} \right), \quad (45)$$

where M_* is the total mass of the pair. We shall stress here that equation (45) provides the *galaxy* merger time-scale, which can be regarded as the time-scale over which a bound SMBH binary forms. The actual coalescence of the binary might be further delayed because the system needs to get rid of its energy and angular momentum in order to get to the efficient GW emission stage. This is known as the ‘final parsec problem’ (Milosavljević & Merritt 2003); we will return on this potential caveat in the next section. The galaxy merger rate is finally obtained by inserting equation (44) – distributing the pairs according to Q^{-1} – and equation (45) into equation (42).

Fig. 6 compares the predicted mass growth and average number of mergers suffered by BCGs as a function of their mass at $z = 1$ to a number of observations and theoretical models. When corrected for the expected contribution of minor mergers, the ‘Fiducial’ model predicts a mass growth in line with observations by Lidman et al. (2012). The ‘Optimistic’ one has a larger growth, consistent with theoretical modelling by De Lucia & Blaizot (2007) and Laporte et al. (2013), whereas the ‘Pessimistic’ is marginally consistent with the data, and tends to slightly underpredict the BCG mass growth (still yielding to mass doubling since $z = 1$). We will consider all models in the following, and we stress that our main results do not qualitatively depend on the details of the growth history of BCGs, so long as most galaxies experience at least one merger at $z < 1$.

A small fraction of our galaxies can grow up to $10^{13} M_{\odot}$ (in the ‘Optimistic’ scenario in particular), which might be at odd with the sharp cut-off in the galaxy mass function observed around $10^{12} M_{\odot}$ (Bell et al. 2003). However, determinations of the mass function are

⁹ We fixed $r_p = 30$ kpc in equation 10 of Kitzbichler & White (2008), because this is the projected separation of the samples we use.

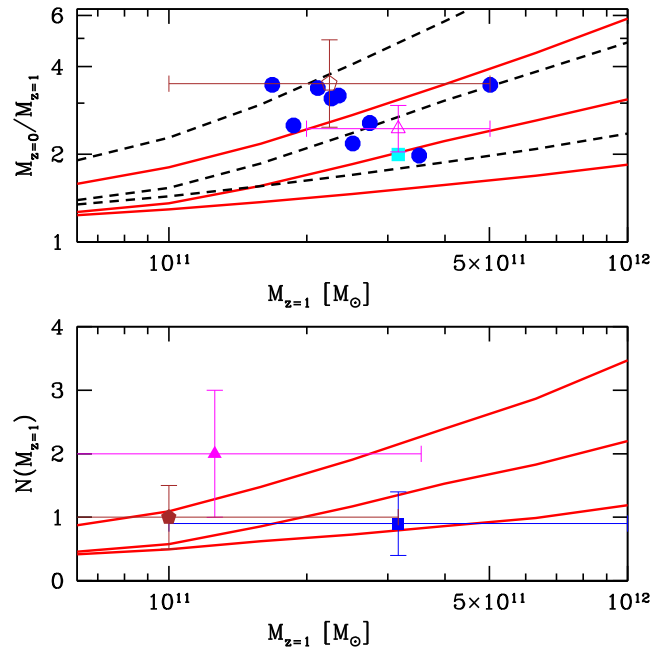


Figure 6. BCG mass growth (top panel) and average number of major mergers (bottom panel) as a function of initial mass at $z = 1$. In both panels, red solid lines are predictions of our observation-based semi-analytic models; from bottom to top: ‘Pessimistic’, ‘Fiducial’ and ‘Optimistic’. In the top panel, the additional black dashed lines are (in the same order) growth factors corrected for the contribution of minor mergers (the lower one corresponds to the ‘Pessimistic-Minor’ model, whereas the same fractional growth correction factor is applied to get the other two curves). The magenta triangle is the average mass growth predicted by Lidman et al. (2012), the brown pentagon is derived from De Lucia & Blaizot (2007), the blue circles are a selected sample of BCGs from Laporte et al. (2013), and the cyan square is a simulation from Oser et al. (2010). In the bottom panel, only the number of major mergers is considered, and we additionally plot the average number of mergers found by Bell et al. (2006, magenta triangle), Xu et al. (2012, brown pentagon) and Hopkins et al. (2010, blue square).

typically obtained by converting luminosities to stellar masses. This results in large systematic uncertainties (especially at the high-mass end) due to the assumptions on the stellar mass-to-light ratio, as well as the different possible light profile fitting procedures (Bernardi et al. 2010), which can extend the high-mass tail of the galaxy mass function by 0.5 dex (Bernardi et al. 2013). Moreover, extreme cases of BCGs with masses possibly in excess of $5 \times 10^{12} M_{\odot}$ have been reported, the most notable case being ESO 146-IG 005 (Carrasco et al. 2010).

2.5 Putting the pieces together

We select the initial BCG mass at $z = 1$ using the high-redshift sample collected by Lidman et al. (2012), consisting in 32 observed BCGs with redshift within 0.8 and 1.6. For each initial galaxy of mass $M_{\text{BCG}} = M_{z=1}$, we assign a number of mergers drawn from a Poissonian distribution with average $N(M_{z=1})$; mass ratios and redshifts of galactic mergers are distributed according to $dN/dz dQ$ as reported in equation (42).¹⁰ Both BCG and each satellite galaxy,

¹⁰ We bin mass and merger distributions and we generate our Monte Carlo samples accordingly. Bin widths have been determined through numerical experiments: 10 bins have been used to map the BCG mass distribution from the Lidman et al. (2012) data; 5 bins have been considered to obtain

are then populated with SMBHs using the SMBH–bulge relation as recently obtained by McConnell & Ma (2013):

$$\log\left(\frac{M_{BH}}{M_{\odot}}\right) = 8.46 + 1.05 \log\left(\frac{M_{BCG}}{10^{11}M_{\odot}}\right), \quad (46)$$

with a dispersion of 0.34 dex. In particular, McConnell & Ma (2013) detect steeper slopes in the galaxy scale laws when BCG data are included in the fitted sample (cf. also Kormendy & Ho 2013). When a BCG merges with a satellite galaxy, we assume that the satellite mass is fully accreted by the BCG:

$$M'_{BCG} = (1 + Q)M_{BCG}. \quad (47)$$

and we compute the stellar and DM profile from M'_{BCG} using the procedure described in Section 2.2. No SMBH remnant can be present in the post-merger BCG if both the parent BCG and satellite did not host any SMBH at their centres; a single SMBH is assumed to lie in the newly formed BCG if only one of the parents carried a SMBH; finally, if both the BCG and the satellites had a SMBH, we assume that the two SMBHs also merge at the same time (redshift) as the galaxies merge. At each SMBH merger, we compute the remnant mass, spin and recoil as presented in Section 2.1. From the kick velocity and the galactic potential of the newly formed BCG, we compute the return time t_R using either t_{DF} from equation (37) or t_B from equation (40) in each of our two models. In practice, the SMBH is removed from the simulation and placed back to the galactic centre after a time t_R . If t_R is smaller than the time between two galactic mergers, the SMBH will simply settle back at the centre of its BCG; if instead a subsequent galactic merger happens before, the BCG centre may already contain a SMBH (coming from one of the satellites). A new binary merger is computed, possibly resulting in another ejection from the BCG.

2.6 Possible caveats

A few simplifying assumptions have been made in the implementation of this procedure, which we justify in the following.

First, we assume that all SMBH binaries merge, thus circumventing the so-called final-parsec problem (Milosavljević & Merritt 2003). The bottleneck to SMBH binary evolution (Begelman et al. 1980) is believed to occur on the parsec scale, where intersecting-orbit stars have all been ejected but GWs are still not efficient enough to finally drive the inspiral. In principle, the relatively low-density gas-poor galaxy cores of BCGs are the most exposed to SMBH binary stalling. It has been found that triaxial potentials might alleviate the problem by increasing the number of orbits that cross the binary’s loss cone, therefore providing a way to get rid of additional binary energy and angular momentum (Merritt & Poon 2004). However, a recent investigation by Vasiliev, Antonini & Merritt (2014) called this result into question by showing that triaxiality alone might not be enough. None the less, in real mergers, other factors such as rotation, bar-like instabilities and an unrelaxed time evolving potential might significantly enhance the flux of stars into the loss cone (Berczik et al. 2006), and recent ab initio N -body simulations of merging stellar bulges succeeded in driving the SMBH binary to final coalescence (Khan et al. 2011; Preto et al. 2011). If some gas is present, this may provide additional help in

the average merger numbers $N(M_{z=1})$ (a Poissonian dispersion is then applied), while for $dN/dz dQ$ we used 4 bins in the mass ratio and 37 bins in the redshift (bin widths are smaller for $z < 0.3$, where redshifts get closer to the end of the simulations $z = 0$).

hardening the binary (see e.g. Armitage & Natarajan 2002; Escala et al. 2005; Dotti et al. 2007 for gas driven binaries), even though it has been also argued that gas might indeed be unable to absorb significant angular momentum from the binary if the gaseous-disc mass is limited by self-gravity and fragmentation (Lodato et al. 2009).

Secondly, we only update SMBH masses and spins during merging events, thus neglecting any accretion mechanism. Giant ellipticals are gas-poor systems, generally unable to supply large amounts of material to feed the central SMBH. It is observationally well known that the accretion activity of the most massive black holes peaks at $z \approx 2$ (see e.g. Hopkins, Richards & Hernquist 2007), rapidly declining at lower redshifts. This trend has been reproduced by state-of-the-art theoretical models, which find that the most massive SMBHs at low z grow primarily via mergers (Malbon et al. 2007; Fanidakis et al. 2011), with little contribution from gas accretion. The change of the SMBH spin magnitude due to accretion can also be safely neglected: momentum-conservation arguments (Thorne 1974) imply that the spin magnitude is modified significantly only if the accreted mass is the order of the SMBH mass itself. This assumption is coherent with taking isotropic spin directions neglecting further spin-alignment processes (see discussion in Section 2.1).

Thirdly, we neglect any delay between galactic and SMBH binary mergers, thus assuming that they take place simultaneously. In reality, binary formation and inspiral will postpone the SMBH merger even if the *final-parsec problem* is solved efficiently. In dense stellar environments, if there is a continuous supply of stars interacting with the binary (technically, a full loss cone) SMBHs generally inspiral for $> 3 \times 10^7$ yr before merging with each other (Sesana 2010), and similar time-scales apply to gaseous environments (Dotti et al. 2009). This delay will likely be longer for low-density ellipticals (Khan et al. 2011); however, BCGs generally experience at most 2–3 major mergers since $z = 1$, therefore delayed SMBH binary mergers could have a substantial impact on our results only if binaries typically survive for Gyr (in which case, the distinction between delayed merger and stalling becomes blurry). We try here to critically assess the impact on delayed mergers on our results. We consider the longest merger time-scales found in N -body simulations of merging galaxies performed by Preto et al. (2011) and Khan et al. (2012). When scaled to massive ellipticals, the results of Khan et al. (2012) give coalescence times that can be as long as ~ 1 Gyr (see their table 5), whereas Preto et al. (2011) provide shorter time-scales (see their fig. 4). We therefore count a posteriori the fraction of subsequent mergers separated by less than 1 Gyr. This fractions turned out to be

- (i) ~ 0.2 in the ‘Fiducial’ scenario;
- (ii) ~ 0.3 in the ‘Optimistic’ scenario;
- (iii) ~ 0.12 in the ‘Pessimistic’ scenario;
- (iv) ~ 0.25 in the ‘Pessimistic-Minor’ scenario (however, in this latter case, also the number of mergers is larger).

We see that delayed mergers can produce triple interaction in 30 per cent of the cases at most (considering only the major merger statistics). When a triplet forms, either (i) a strong triple interaction occurs, causing the ejection of the lightest of the three SMBHs (and possibly accelerating the coalescence of the binary left behind), or (ii) a hierarchical system forms, possibly exciting Kozai resonances in the inner binary, again driving it to rapid coalescence. The outcome of the two processes is generally different, and the occurrence of one or the other depends on how far has the SMBH binary already gone into the hardening process, on how shallow

has the galaxy core became, etc. We notice, however, that in case (i) the number of coalescences decreases at most proportionally with the fraction of triplets that forms, whereas in case (ii), the number of coalescences is basically unaffected, since each triplet formation leads to the coalescence of the binary that was already in place. Extensive numerical experiments performed by Hoffman & Loeb (2007) showed that triple interactions generally lead to at least one binary coalescence (in 85 per cent of the cases), usually on a time-scale shorter than 1 Gyr (fig. 8 in Hoffman & Loeb 2007). Therefore, triple interactions might cause a fractional change of our ejection fractions of 0.3 at most. In any case, it might be interesting to track consistently triplets in our simulations, and this point may be the subject of future improvements of our model. We also note that similar assumptions are also often made in more elaborate galaxy-evolution models (see e.g. Barausse 2012 for a critical discussion).

We are also neglecting the previous merger history of the BCGs. BCGs will generally reach $z = 1$ after multiple merger events. The inspiral of a SMBH binary preceding a merger is expected to leave an imprint on the host galaxy in the form of a core scouring in the BCG centre (especially if little nuclear star formation occurs). At each merger, the mass ejected in stars is of the order of $\sim 0.5M$ (where M is the total mass of the binary; Merritt 2006). The effect may be important after many merger generations and it leads to strong modification of the galactic potential in the core region. This effect is absent in our simplified model, but we note that the core properties are only important when estimating the SMBH return time in the Bounce model (Section 2.3). The fitting procedure developed here is built on the results obtained by Gualandris & Merritt (2008), which in turn consider an elaborate galaxy model (Terzić & Graham 2005) where core depletion is taken into account.

3 RESULTS AND DISCUSSION

We combine different prescriptions for two main processes:

- (i) the return time: Dynamical friction or ‘Bounce’ (Section 2.3);
- (ii) the merger distribution: ‘Fiducial’, ‘Optimistic’ or ‘Pessimistic’ (Section 2.4).

This results in a set of six models that we use as investigation playground: ‘Fiducial-DF’, ‘Fiducial-Bounce’, ‘Optimistic-DF’, ‘Optimistic-Bounce’, ‘Pessimistic-DF’, ‘Pessimistic-Bounce’. In each model, the evolution of the SMBH population is characterized by the following input parameters:

- (i) initial BCG occupation fraction $f_{z=1}$;
- (ii) occupation fraction of the satellite galaxies f_s ;
- (iii) initial SMBH spin magnitudes in the BCGs $\chi_{z=1}$;
- (iv) SMBH spin magnitudes in the satellites χ_s .

We discuss in the following the results of our simulations, separating the effect of each individual parameter. The main observables are

- (i) final BCG occupation fraction $f_{z=0}$ (later split between those galaxies which underwent a SMBH replenishment $f_{z=0}^R$ and those which keep their original SMBH $f_{z=0}^{NR}$);
- (ii) fraction of BCG that do not host a nuclear SMBH at $z = 0$, simply defined by $1 - f_{z=0}$;
- (iii) distance from the BCG centre (offset) of the ejected SMBH at the present time $r_{z=0}$.

For any given set of parameters, we simulate 1000 BCGs (with the exception of the runs presented in Figs 9 and 11 which contains 10000 BCGs): typical Poisson counting errors on the final

occupation fractions are therefore ~ 3 per cent. Most of the results presented here (with the exception of Section 3.2.2 where such issue is explicitly investigated) are computed assuming $f_{z=1} = 1$ as a simplifying assumption (cf. Section 1)

3.1 The impact of the host properties: cluster shape and BCG merger rates

The six models described above are defined by distinct ‘environmental properties’ which are not directly related to the SMBH population itself; namely the merger history of BCGs (determining the number of SMBH binary mergers) and the shape of the cluster potential (governing the typical return time-scales of ejected SMBHs). We describe their impact on the results first (fixing $f_{z=1} = f_s = 1$), turning to the properties of the SMBH population in the next subsection.

3.1.1 Bounce versus DF models

The detailed shape of the cluster potential affects the trajectory of the recoiling SMBH. If all gravitational potentials were spherically symmetric, then SMBHs would always get back to the core of BCGs, and the Bounce model would provide a complete description of the dynamics. However, cluster density profiles are often triaxial, unrelaxed, and ‘clumpy’. In a triaxial potential orbits do not conserve angular momentum, implying that the SMBH will miss the BCG core at subsequent passages; additionally, gravitational perturbations due to subhaloes and other galaxies can easily deflect the SMBH out of its initially radial orbit. The DF model is taken as an extreme (and admittedly unrealistic) case in which the SMBH returns on a circular orbit. Both the DF and the Bounce models are idealizations meant to bracket the range of possible outcomes. As shown in Fig. 4 for three selected systems, return time-scales can easily exceed the Hubble time in the DF model. This is better seen in Fig. 7 where the distributions of recoil velocities v_k and return times t_R are computed along the evolution of the BCG population for our four default models. For all of them, the recoil distribution presents a high-velocity tail extending to about 4000 km s^{-1} , with a median value of about 600 km s^{-1} . The difference between the Bounce and the DF models is clearly shown in the return time distribution. As expected, the rise of the distribution at $t_R < 1 \text{ Gyr}$ (corresponding to small kick velocities) is similar because the bounce dynamics is basically equivalent to a DF process when the SMBH do not leave the galaxy core. However, in the DF scenario, about 10 per cent of the SMBH are ejected outside the host BCG and interacts only with the low-density DM background outside the galaxy, with resulting return times longer than 10 Gyr (cf. the bump of the black distributions in the left-hand panel of Fig. 7). As a result, BCG occupation fractions $f_{z=0}$ can be as low as 85 per cent in the case $\chi_{z=1} = \chi_s = 1$, as reported in the upper panels of Fig. 8. Conversely, in the Bounce model, only few SMBHs do not make it back to the galaxy core following a kick, resulting in occupation fractions of 98 per cent or higher. The two models are best compared in terms of ‘depleted fraction’, i.e. the fraction of BCGs that do not host a SMBH at $z = 0$, which is simply $1 - f_{z=0}$. This is shown in the lower panels of Fig. 8; it is clear that the DF model depletes BCGs of their central SMBH 10 times more efficiently than the Bounce model.

3.1.2 Fiducial, optimistic and pessimistic models

Conversely, the adopted merger rate does not have a strong impact on $f_{z=0}$, and the difference between Fiducial, Optimistic and

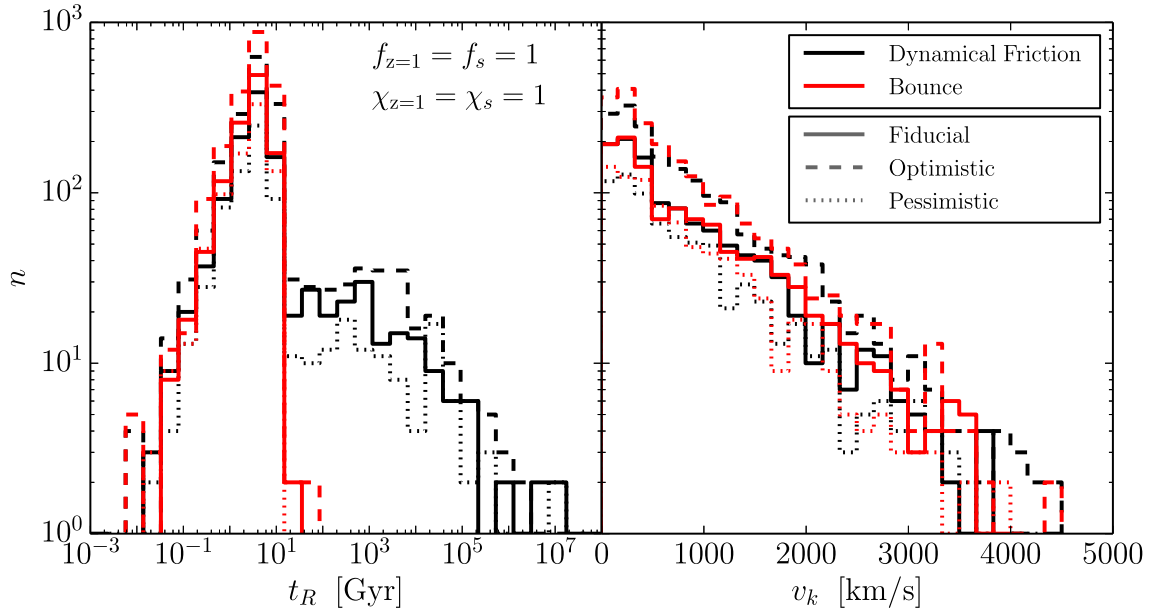


Figure 7. Return time distribution t_R (left) and recoil velocity distribution v_k (right) of all kicked SMBH in a 1000-events Monte Carlo realization of our four fiducial models. Red (black) curves are for the Bounce (DF) models, whereas solid, dashed and dotted curves correspond to the Fiducial, Optimistic and Pessimistic scenarios respectively, as labelled in figure. The dotted vertical lines are the median values of all the distributions (which are not distinguishable on this scale). All distributions are computed assuming unity occupation fractions at $z = 1$ and $\chi_{z=1} = \chi_s = 1$.

Pessimistic models is only modest, being at most a factor of ~ 2 in terms of depleted fractions, as shown in Fig. 8. For example, for $\chi_{z=1} = \chi_s = 1$, $1 - f_{z=0}$ varies between 0.1 and 0.15. The impact of minor mergers is also small, as shown in the left-hand panels of Fig. 8.

Although apparently counter intuitive, this result is in fact expected because a higher BCG merger rate implies also a higher probability of multiple mergers. While it is true that each SMBH has a larger chance to be kicked out of its host, it is also true that there is a higher probability that it is replaced by another (possibly undermassive) SMBH brought in by a subsequent merger. Enhanced ejections and replenishments nearly cancel out making $f_{z=0}$ only weakly dependent on the details of the merger history. This is illustrated in Fig. 9, where the extreme case $\chi_{z=1} = \chi_s = 1$ is considered. In the Fiducial-DF model, 87 per cent of the BCGs host a SMBH at $z = 0$ ($f_{z=0} = 0.87$); however, only 79 per cent of them retained their original $z = 1$ SMBH, while ~ 9 per cent are depleted of their original SMBH and ‘replenished’ in a subsequent merger with a satellite galaxy hosting a SMBH. In the Optimistic-DF model those percentages become 69 and 16 per cent, respectively: more SMBH are ejected (only 69 per cent of original SMBHs retained), but a larger fraction of BCGs is replenished (16 per cent) by virtue of the higher merger rate (causing a higher probability of multiple mergers). The opposite behaviour is detected when the Pessimistic-DF scenario is considered. The balance is almost perfect in the Bounce models (also shown in Fig. 9). All three scenarios show $f_{z=0} \simeq 0.98$, but the probability of replenishment increases from the Pessimistic to the Fiducial and Optimistic models following a larger number of SMBH ejections.

As expected, the SMBH-mass distributions are different for replenished and non-replenished galaxies. Non-replenished galaxies reflect the injected correlation law (equation 46) with lower scattering at $z = 0$, while the replenished samples tend to host undermassive SMBHs which have grown within smaller satellite galaxies in the cluster.

3.2 The impact of the SMBH properties: spin magnitude and initial occupation fraction

Having explored the impact of the physics governing the evolution of the SMBH environment, we turn now to a description of the effect of the parameters related to the SMBH population itself; in particular SMBH spins and initial occupation fraction.

3.2.1 Spin magnitude

The magnitude of the SMBH spin vectors in BCGs is essentially unknown, since most of the direct measurements from $K\alpha$ iron lines involve local Seyfert galaxies (Brenneman 2013; Reynolds 2013) and it is difficult to derive clear constraints through indirect arguments related to jet production, AGN spectra energy distribution fitting, or the evolution of the SMBH accretion efficiency with mass and redshift (see e.g. Wang et al. 2009; Shankar et al. 2010; Netzer & Trakhtenbrot 2014). However, we know that spins are crucial in the physics of gravitational recoils, because highly spinning SMBHs are likely to experience stronger recoils (see equation 14). We therefore need to investigate the SMBH parameter space carefully, to cover the full range of possibilities predicted by our models. For each of our four models, we initialize $\chi_{z=1}$ at a fixed value, running between zero and one. As stated in Section 2.1, the spin orientations are assumed to be isotropic. For each case, we consider two different χ_s distributions: (i) $\chi_s = \chi_{z=1}$ in each individual merger, and (ii) χ_s random in the range $[0, 1]$. As shown in the upper panels of Fig. 8, $f_{z=0}$ is always a decreasing function of $\chi_{z=1}$, and is fairly well described by a quadratic function. Trends are best seen in the lower panels of Fig. 8, where we plot the depleted BCG fraction $1 - f_{z=0}$. In terms of the depleted fraction, spins have an order of magnitude impact on the results. In the DF model, only ≈ 1 –4 per cent of the BCGs are depleted at $z = 0$ (i.e. $1 - f_{z=0} = 0.01$ – 0.04) for $\chi_{z=1} = 0$, whereas up to ≈ 10 –15 per cent of the BCGs lost their SMBH at $z = 0$ (i.e. $1 - f_{z=0} = 0.1$ – 0.15) for $\chi_{z=1} = 1$.

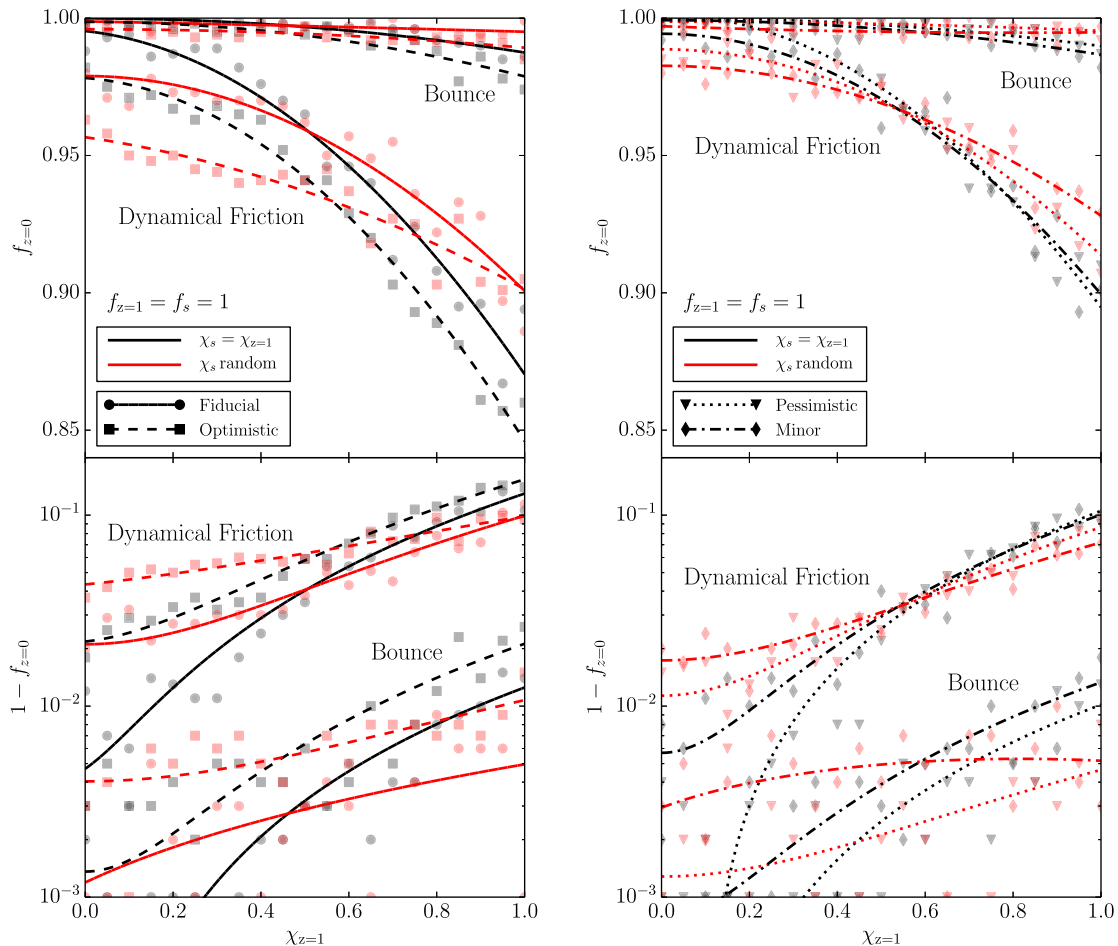


Figure 8. BCG occupation fractions. The left-hand plot shows the ‘Fiducial’ and the ‘Optimistic’ models, whereas the right-hand plot compares the ‘Pessimistic’ and the ‘Pessimistic-Minor’ models, to assess the impact of minor mergers. In each plot, the top panel shows the dependence of the $z = 0$ occupation fraction $f_{z=0}$ on the initial BCG spin magnitude $\chi_{z=1}$. To highlight the peculiarities of each individual model, the lower panel shows the corresponding depletion fraction $1 - f_{z=0}$, in logarithmic scale. Runs have been performed with two prescriptions on the spin magnitude of the satellite galaxy SMBHs χ_s , taken either to be equal to the spins of the BCG SMBHs (black curves) or uniformly distributed in $[0, 1]$ (red curves). A quadratic interpolation is presented in both cases. While final fractions as low as ~ 0.85 are detected in the DF scenario, only $f_{z=0} \sim 0.98$ can be achieved in spherically symmetric (Bounce) galaxies even for maximally spinning SMBHs.

Similar trends hold for the Bounce model, but in that case only ≈ 0.1 per cent to ≈ 2 per cent of the SMBHs are lost at $z = 0$. It is interesting to notice that even for $\chi_{z=1} = 0$, we get $0.01 < 1 - f_{z=0} < 0.04$ in the DF models. This is, again, because of multiple mergers: a Schwarzschild SMBH can acquire a spin $\chi \approx 0.5\text{--}0.6$ in a single merger event (see equation 9), which significantly enhances the probability to experience a superkick if a subsequent merger occurs. The different χ_s prescriptions (case i and ii above) show the same qualitative feature. The fits to the depleted fractions (lower panel of Fig. 8) intersect around $\chi_{z=1} = 0.5$ as expected: for lower values, the average χ_s in case (ii) is larger, resulting in more superkicks and more SMBH ejections, while the opposite is true in case (i).

3.2.2 Initial BCG occupation fraction

All theoretical models developed to reproduce the SMBH cosmic evolution (including present number density, and quasar luminosity function up to high redshift) require an amount of SMBHs that guarantees an occupation fraction $f = 1$ for massive galaxies (see e.g. Malbon et al. 2007; Bellovary et al. 2011; Guo et al. 2011; Khandai

et al. 2014), pending, of course, the occurrence of superkicks. There is always the possibility that a superkick occurs at $z > 1$, even though galaxies at higher redshift are generally richer of cold gas, which will likely promote SMBH spin alignment during mergers (Bogdanović et al. 2007; Dotti et al. 2010), ultimately suppressing superkicks (Kesden et al. 2010b). None the less, this might introduce some uncertainty on $f_{z=1}$ and, although we do not expect it to be far from unity, we study the sensitivity of our models to this parameter for completeness.

Fig. 10 shows $f_{z=0}$ as a function of $f_{z=1}$, for 240 different merger trees. The main evidence is that $f_{z=1}$ scales linearly with $f_{z=0}$. The slopes and the intercept of the linear relation mostly depend on the occupation fraction of the satellite galaxies f_s , i.e. on how many SMBHs are injected in the simulations between $z = 0$ and $z = 1$. The linear relationship between $f_{z=1}$ and $f_{z=0}$ can be easily understood using a simple analytic model (built on the line of Schnittman 2007). The probability f_i of a BCG to have a SMBH at the i th merger generation consists in the sum of (i) the probability that only the BCG had a SMBH at the previous generation $f_{i-1}(1 - f_s)$, (ii) the probability that only the satellite had a SMBH $f_s(1 - f_{i-1})$ and (iii) the probability that there has been a merger but the SMBH has not

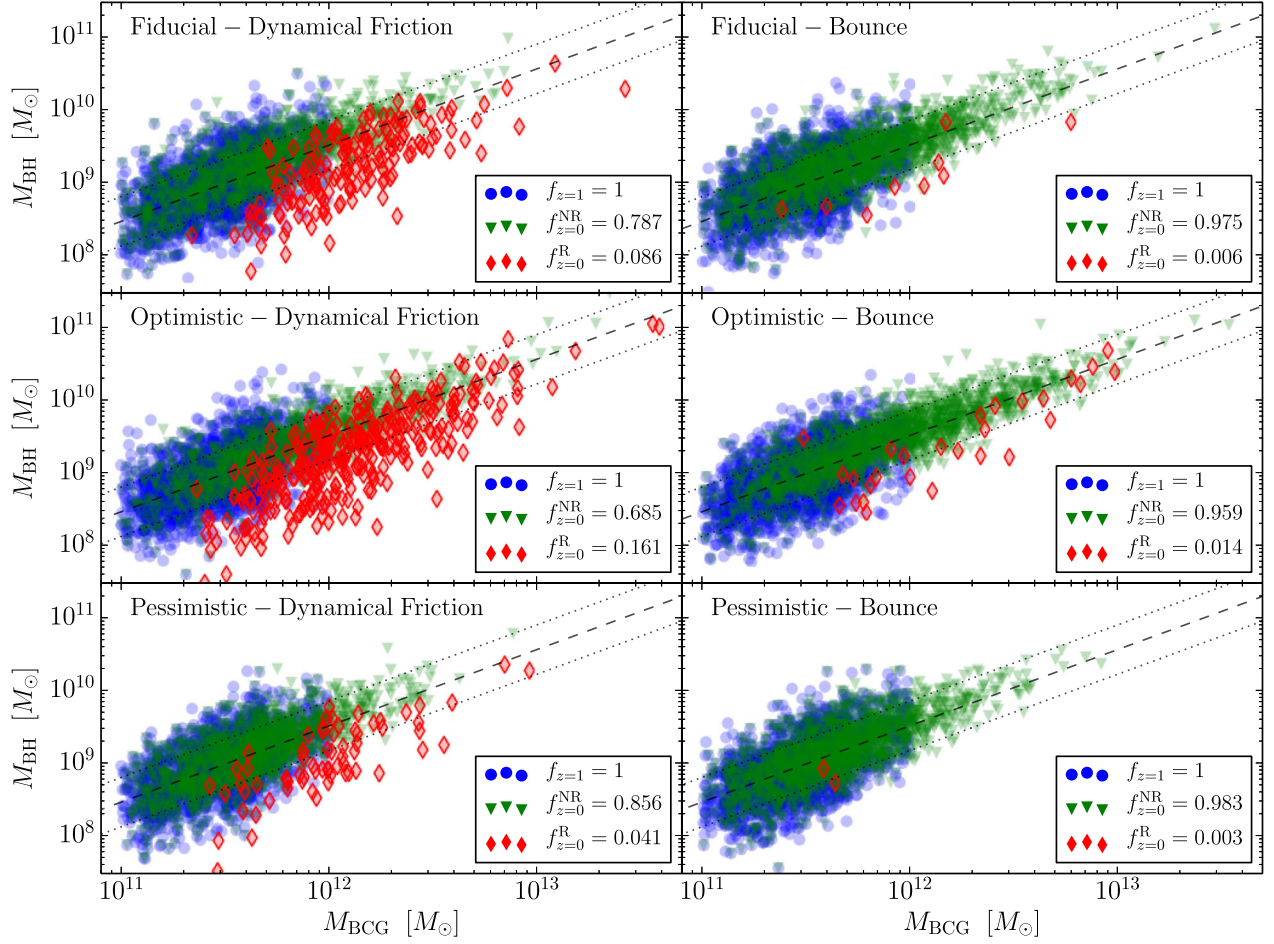


Figure 9. Deviations from the SMBH/host relation in replenished galaxies, and final occupation fractions. We show the distributions of the SMBH mass M_{BH} and the galaxy mass M_{BCG} in our six different models, assuming $f_{z=1} = f_s = 1$ and $\chi_{z=1} = \chi_s = 1$. Dashed and dotted lines show the average and the standard deviation of the initial correlation (equation 46). Blue circles shows the initial $z = 1$ sample. We track those system where a replenishment occurred (R, red diamonds) and those which just underwent a plain evolution to $z = 0$ (NR, green triangles). While the evolved NR sample still lies on the $z = 1$ correlation but with lower scatter, replenished galaxies clearly exhibit deviations towards lower M_{BH} values. Occupation fractions for each sample are reported in the legends and are computed considering 10000 initial BCGs; points are shown for only 2000 initial BCGs to avoid cluttering.

been ejected $f_s f_{i-1} (1 - P_{\text{ej}})$ (where P_{ej} is the ejection probability). This yields

$$f_i = f_s + f_{i-1} - f_s f_{i-1} (1 - P_{\text{ej}}). \quad (48)$$

Using the convergence limit $f_\infty = 1/(1 + P_{\text{ej}})$, and fixing $f_{z=1}$ as initial condition, we can write down the previous expression as a geometric progression:

$$f_i - f_\infty = (f_{z=1} - f_\infty) \left(1 - \frac{f_s}{f_\infty}\right)^i. \quad (49)$$

With the further (strongly idealized) assumption that P_{ej} is constant over different merger generations, we can estimate the final occupation fraction in our samples to be

$$f_{z=0} - f_\infty = (f_{z=1} - f_\infty) \sum_{j=0} \epsilon_j \left(1 - \frac{f_s}{f_\infty}\right)^j, \quad (50)$$

where ϵ_j is the fraction of BCG in which j mergers occur between $z = 1$ and 0. The above expression confirm the main trends observed in the simulations presented in Fig. 10, namely the linear relationship between $f_{z=0}$ and $f_{z=1}$, with slope and intersect mainly depending on f_s . The initial occupations $f_{z=1}$ and f_s are

physically determined by cosmic history at early times ($z > 1$), whose modelling is outside the scope of the present paper. However, as discussed before, we expect any deviation of $f_{z=1}$ from unity to be also related to the occurrence of superkicks.

3.3 Discussion

Our results show that superkicks likely have very interesting and potentially observable astrophysical consequences, most notably, a decrease of the SMBH occupation fraction in BCGs down to 0.9 or lower, under specific assumptions. At the time of writing, secure SMBH mass measurements have been performed in about 10 BCGs (McConnell et al. 2012), an insufficient number to empirically constrain the models presented here. As described in the introduction, future thirty-metre-class telescopes like ELT and TMT can easily boost those figures by a factor of 10 or more. With $\mathcal{O}(100)$ SMBH mass measurements, significant deviations from $f_{z=0} = 1$ can be measured, making possible to directly test our superkick models, and possibly providing insights on the BCG SMBH spin distribution. As shown in the previous section, $f_{z=0}$ strongly depends on both spin magnitudes and the detailed shape of the cluster potentials. The effect of the two ingredients is somewhat degenerate, since both

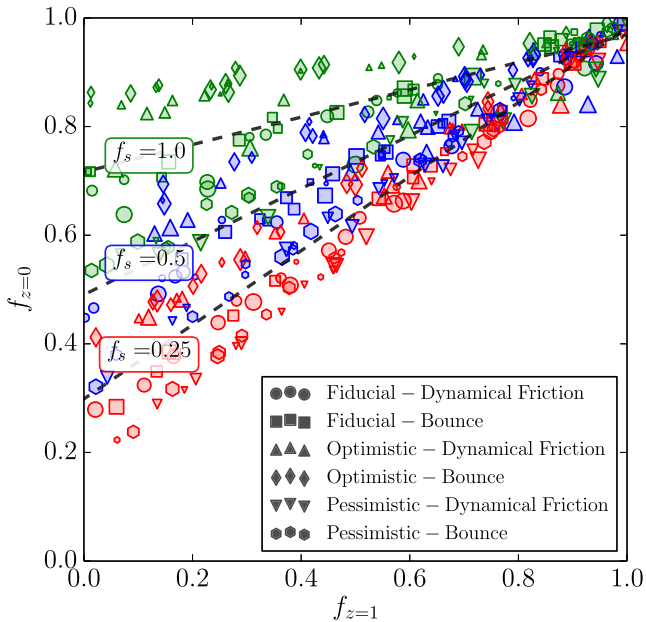


Figure 10. Dependence of the final BCG occupation fraction ($f_{z=0}$) on the initial occupation fraction of BCGs ($f_{z=1}$) and satellites (f_s). Each point represents a simulation of 1000 clusters where both the initial BCG and the satellite galaxies have the same initial spin $\chi_{z=1} = \chi_s$ (indicated with symbol size, where small symbols stand for slowly rotating SMBHs and large symbols for high spins) and model prescriptions (indicated with different symbol shapes, as detailed in the legend). Each sample (clustered along the dashed lines, with different colours) is computed with a different value of f_s . As confirmed analytically, the final BCG occupation fraction scales linearly with the initial occupation fraction; slopes and intercept are mainly determined by f_s .

high spins and non-spherical potentials tend to reduce the occupation fraction. The degeneracy is, however, only partial. For example, $f_{z=0} < 0.9$ is possible only if cluster potentials are extremely non-spherical *and* typical spins are higher than 0.8. A measurement of such low BCG occupation fraction will therefore provide valuable information on both the dynamics of the kicked SMBHs and their spins. Conversely, an occupation fraction of, say, 0.98 can be due to a combination of extremely low spins and non-spherical potentials *or* very high spins and almost spherical potentials, as demonstrated in the lower panel of Fig. 8. In this case, degeneracy might be broken via independent measurements of the cluster mass distribution derived, for example, by lensing. Those allow us to reconstruct the shape of the cluster potential, thus providing an estimate of how likely/unlikely it is for an ejected SMBH to return on a radial orbit.

We note that the Bounce and DF prescriptions have been taken as extreme cases of a continuum range of possibilities. Since those prescriptions have a strong impact on the results, we can try to assess which of the two might be closer to reality on the basis of qualitative theoretical arguments. In the Bounce model, subsequent passages of the SMBH across the BCG core are crucial in damping the radial oscillations, critically shortening the return time. As a matter of fact, the clumpiness of a typical galaxy cluster mass distribution might easily cause a SMBH kicked to a few hundred kpc to miss a galaxy core which is smaller than 10 kpc across (Lauer et al. 2007). A simple estimate of the deviation from the radial path can be done by considering close encounters between the kicked SMBH and other cluster galaxies at apoastron. Consider a SMBH ejected at $r \approx 100$ kpc in a typical cluster of $M_{\text{DM}} = 5 \times 10^{14} M_{\odot}$. The typical time it spends close to apoastron is $\delta t \approx 0.1$ Gyr. The gravitational

pull of a galaxy with mass M at a distance d from the SMBH, will cause a velocity change

$$\delta v \approx \frac{GM}{d^2} \delta t \approx 50 \left(\frac{M}{10^{10} M_{\odot}} \right) \left(\frac{d}{10^4 \text{ pc}} \right)^{-2} \text{ km s}^{-1}. \quad (51)$$

In a galaxy cluster like Coma, the galaxy density at 100 kpc from the centre is few times 10^3 galaxy Mpc^{-3} (Weinzirl et al. 2014), implying that the presence of at least one perturber at $d < 10$ kpc is guaranteed. Considering a circular velocity of $v_c \approx 10^3$ km s^{-1} , it is therefore very likely that SMBHs kicked at $r > 100$ kpc will acquire a tangential velocity component $\approx 0.1 v_c$ because of interactions with nearby cluster galaxies (and clumpiness of the DM halo). We performed a simple test of the DF return time-scales for non-circular orbits by numerically integrating the DF equations in a Hernquist+NFW potential. We placed the sinking SMBH at a distance R from the centre, and we gave it an initial velocity $v = v_c(R)$ and $v = 0.1 v_c(R)$. The first case corresponds to a circular orbit, while the second implies a nominal eccentricity of $e \approx 0.98$ (if the orbit was Keplerian). Despite an almost radial orbit, the return time-scale in the latter case was only approximately five times shorter. We tested that reducing t_{DF} in equation (37) by a factor of 5 may cause a maximum variation of ~ 0.07 on $f_{z=0}$ in the extreme case $\chi_s = \chi_{z=1} = 1$, which still implies $f_{z=0} \approx 0.9$. This suggests that small deviations from a perfectly radial orbit result in return time-scales just a factor of a few smaller than our DF computation, but two orders of magnitude longer than the Bounce model prediction, which is therefore relevant only for almost spherical potentials. We conclude that the DF scenario provides a better approximation for the return time-scales in realistic potentials implying interesting observational prospects. As shown in Fig. 8, a DF-like dynamics results in $f_{z=0} < 0.99$ for basically any choice of other relevant parameters, and the superkick effect should be detected with a sample of $\mathcal{O}(100)$ SMBH mass measurements.

Besides the lower BCG occupation fraction, another interesting phenomenon is BCG replenishment. We saw in the previous section that depleted BCGs can be replenished in a subsequent merger with another SMBH carried by the satellite galaxy. In this case, the new SMBH will most likely be undermassive with respect to the BCG mass. This is shown by the red diamonds in Fig. 9, which lie ≈ 0.3 dex below the SMBH–bulge relation defined by the green triangles. However, the net effect of replenishment is just to produce a slightly lower normalization and larger scatter in the SMBH–bulge relation, which would be hard to identify observationally.

The implications of superkicks on the BCG occupation fraction are directly mirrored in the presence of a complementary population of wandering SMBHs. In fact, as already noted, full ejections from galaxy clusters are extremely unlikely because of the high escape speeds. As a natural consequence, some recoiled SMBHs are still sinking back to the BCG centre today, and can potentially be detected as off-centre objects, adding evidence to the superkick scenario. Because of the longer return time-scales, off-centre SMBHs are expected to be at least 10 times more likely in the DF than in the Bounce models. The offset distribution is shown in Fig. 11 for three values of the the spin magnitudes $\chi_{z=1} = \chi_s = 0, 0.5, 1$, assuming the ‘Fiducial’ model (other models, not shown, yield similar results). The absolute number of recoiling SMBHs in each panel is directly related to the average kick velocity imparted after SMBH mergers, which reflects the average spin magnitude. Distributions are generally monotonically decreasing functions of the offset $r_{z=0}$, meaning that many of these wandering SMBHs are concentrated in a few central kpc. However, in the maximally spinning case (right-hand panel) about 50 per cent of the ejected SMBHs are located

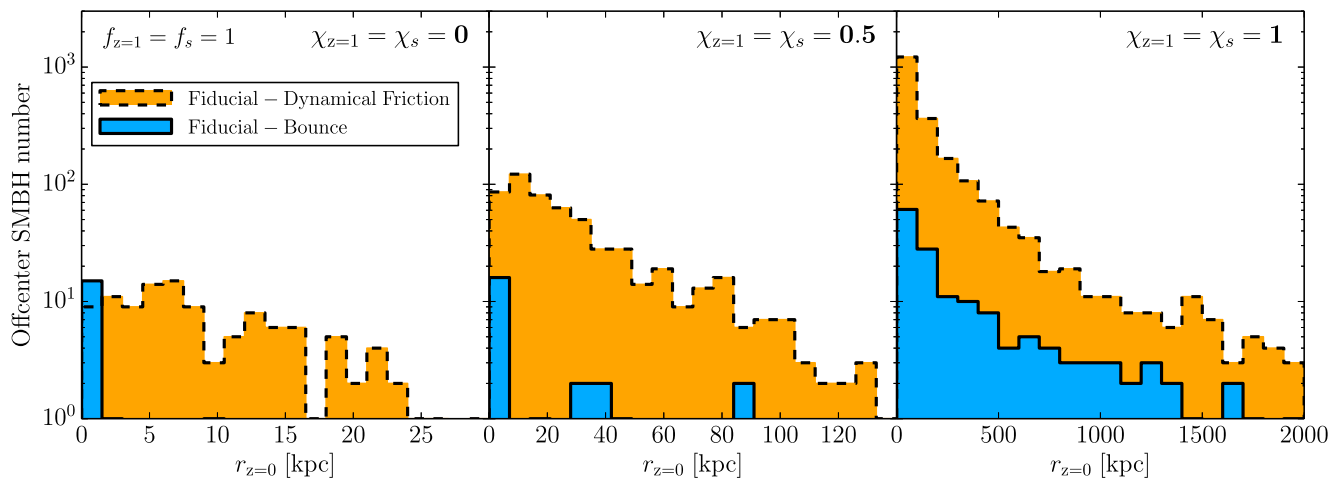


Figure 11. Number of wandering, off-centre, SMBHs as a function of their present distance from the galactic centre (offset) $r_z=0$. The DF models (suited for non-spherical potentials) present at least a factor ~ 10 more wandering SMBHs than the Bounce models. SMBH detection through off-nuclear quasar signatures or compact stellar systems may therefore distinguish between the two scenarios. Each run presented in this figure contains 10000 BCGs, which sets the absolute scale of the SMBH number; three different spin-magnitude values $\chi_{z=1} = \chi_s = 0$ (left-hand panel), 0.5 (middle panel) and 1 (right-hand panel) are considered; initial occupation fractions are fixed at $f_{z=1} = f_s = 1$.

well outside the central BCG, with an offset between 100 kpc and 1 Mpc. Moreover, a tail extending to few Mpc is present, implying that a few SMBHs might even lurk in the outskirts of galaxy clusters. For this favourable configuration, we predict that between 0.5 and 5 per cent of massive galaxy clusters should host a wandering BCG SMBH with an offset of a few hundred kpc from the cluster centre. The situation is less promising for lower spin values, even though in the intermediate case (central panel) for the DF model, about 1 per cent of the BCGs might host SMBHs lurking at few tens of kpc from their centres.

Several observational signatures of recoiling SMBHs have been proposed in the literature, ranging from off-centre AGNs (Blecha et al. 2011) and tidal disruptions (Komossa & Merritt 2008; Li et al. 2012), to intracluster ultracompact stellar systems (Merritt, Schnittman & Komossa 2009). All of them rely on the fact that the recoiling SMBH is carrying with it a significant amount of nuclear gas and stars, which is not likely in our case. First, BCGs are mostly gas-poor systems with shallow stellar cores; little cold gas should be available in the surrounding of the merger remnant, disfavours off-nuclear AGN activity. Secondly, the SMBH can carry away only material that is orbiting around it with a velocity greater than the kick velocity v_k . Ejections to a few hundred kpc require $v_k > 1500 \text{ km s}^{-1} \gg \sigma$, implying that the mass in stars and gas that can be carried away is likely < 1 per cent of the SMBH mass. Lastly, because of their high mass, those SMBHs will simply swallow stars without tidally disrupting them, inhibiting the tidal disruption channel as a possible observational signature. The only possibility seems therefore to be the challenging detection of a faint ultracompact cluster with extremely high velocity dispersion, which might be feasible in nearby galaxy clusters as discussed by Merritt et al. (2009). Alternatively, also ‘naked’ SMBHs still interact with the diffused hot intracluster gas. This can produce X-ray emission potentially observable at nearby galaxy cluster distances (see Devecchi et al. 2009 for details).

4 SUMMARY AND CONCLUSIONS

In this paper, we investigated the consequences of superkicks for the population of the most massive SMBHs in the Universe residing in

BCGs. The choice of BCGs as study targets follows from a number of theoretical and observational arguments: (i) compared to other types of galaxies, BCGs have the richest merger history, especially at low redshift, (ii) future thirty-metre-scale telescopes will have the resolution to easily reveal SMBHs in hundreds of BCGs up to $z \approx 0.2$, (iii) theoretically, BCGs are expected to have unit SMBH occupation fraction, and even a single depleted system would be the smoking gun of superkick occurrence in nature. We demonstrate that, under plausible astrophysical assumptions, SMBHs can be ejected from BCG cores, potentially resulting in an occupation fraction substantially lower than one in the local Universe (say, $z < 0.1$).

Starting from the observational fact that BCGs have doubled their mass since $z = 1$ – and that this mass growth is consistent with their merger activity as inferred from galaxy pair counts, and as found in simulations of galaxy formation – we have constructed a simple semi-analytical model to track their evolution to the present time. Our model reconstructs the dynamics of each single major merger, including a self-consistent computation of the gravitational recoil and of the return time of the kicked SMBHs. We considered six classes of models combining two BCG major merger history models (‘Fiducial’, ‘Optimistic’ and ‘Pessimistic’, covering the range consistent with observations and simulations) and two specific prescriptions for the return times (‘Bounce’ and ‘DF’). Minor merger rates were also available for the ‘Pessimistic’ scenario, we investigated their impact by including them in the ‘Pessimistic-Minor’ model. Since the magnitude of the spins of SMBHs in BCGs is basically unknown, for each model we considered a range of spin distributions for the SMBHs residing in the BCGs, χ , and in the merging satellites, χ_s . We ran several sets of simulations varying all the relevant parameters, we studied their impact on the final BCG occupation fraction $f_{z=0}$, and we investigated possible observational consequences.

Our main results can be summarized as follows:

- (i) superkicks can efficiently deplete BCGs of their central SMBHs. The occupation fraction at $z = 0$ can be as low as $f_{z=0} = 0.85$ for the most favorable scenarios;

(ii) $f_{z=0}$ is quite insensitive to the BCG merger history, so long as those experience at least ≈ 1 merger since $z = 1$;

(iii) only small quantitative differences were found when comparing the ‘Pessimistic’ and the ‘Pessimistic-Minor’ models, implying that the poorly constrained distribution of minor mergers is not a significant caveat to our findings;

(iv) $f_{z=0}$ is very sensitive to the dynamics of the ejected SMBHs in the galaxy cluster potential well. The fraction of depleted BCGs (i.e. $1 - f_{z=0}$) is of the order of 0.01 only for the Bounce models, but it is typically 0.05–0.1 for the DF models;

(v) the initial value of the SMBH spins has an order of magnitude influence on the depleted BCG fraction. In the DF models, this varies from ≈ 0.02 for non-spinning SMBHs, up to ≈ 0.15 for maximally spinning SMBHs;

(vi) we predict that a few per cent of the galaxy clusters host an offset BCG SMBH inspiralling at a few hundred kpc from the dynamical centre, although they might be extremely difficult to detect;

(vii) for a large variety of physically plausible scenarios, we predict $f_{z=0} < 0.99$, that can be directly tested with measurements of SMBHs in the centre of $\mathcal{O}(100)$ BCGs with future thirty-metre telescopes.

As detailed in Section 2.5, we made a number of simplifying assumptions in our calculation. In particular, we neglected any possible mass and spin evolution due to gas accretion, and we assumed SMBH binaries always merge following galaxy mergers (i.e. we bypassed the *final parsec problem*). Moreover, we assumed random spin orientations when computing kick velocities. We showed that all these assumptions are well justified at least for the majority of mergers involving BCGs, but refinement of some of them might be considered for future work.

Although current statistics of SMBH mass measurements in BCGs is insufficient to empirically constrain the models presented here, prospects look promising for the next generation of thirty-metre-class optical telescopes. Any measurement of a BCG occupation fraction lower than unity will provide observational evidence for the occurrence of superkicks in nature, bringing the extreme dynamical effects of strong-field general relativity to the realm of observational astronomy.

ACKNOWLEDGEMENTS

We thank Emanuele Berti, Ulrich Sperhake, Giovanni Rosotti, Enrico Barausse, Tod Lauer, Marc Postman and Christopher Reynolds for helpful discussions. DG is supported by the UK Science and Technology Facility Council and the Isaac Newton Studentship of the University of Cambridge; partial support is also acknowledged from the FP7-PEOPLE-2011-CIG Grant No. 293412 ‘CBHEO’; the FP7-PEOPLE-2011-IRSES Grant No. 295189 ‘NRHEP’; the STFC GR Roller Grant No. ST/L000636/1; the Cosmos system, part of DiRAC, funded by STFC and BIS under Grant Nos. ST/K00333X/1 and ST/J005673/1; the NSF XSEDE Grant No. PHY-090003; the CESGA-ICTS Grant No. 249 and the NSF CAREER Grant No. PHY-1055103. AS is supported by the DLR (Deutsches Zentrum für Luft- und Raumfahrt) through the DFG grant SFB/TR 7 Gravitational Wave Astronomy. DG finally thanks the kind hospitality received at the AEI where this work was conceived. Most figures have been generated using the PYTHON-based MATPLOTLIB package (Hunter 2007).

REFERENCES

- Armitage P. J., Natarajan P., 2002, *ApJ*, 567, L9
 Ascaso B., Lemaux B. C., Lubin L. M., Gal R. R., Kocovski D. D., Rumbaugh N., Squires G., 2014, *MNRAS*, 442, 589
 Baker J. G., Centrella J., Choi D.-I., Koppitz M., van Meter J., 2006, *Phys. Rev. Lett.*, 96, 111102
 Barausse E., 2012, *MNRAS*, 423, 2533
 Barausse E., Rezzolla L., 2009, *ApJ*, 704, L40
 Barausse E., Morozova V., Rezzolla L., 2012, *ApJ*, 758, 63
 Bardeen J. M., 1973, in Dewitt C., Dewitt B. S., eds, *Black Holes (Les Astres Occlus)*. Gordon and Breach, New York, p. 215
 Begelman M. C., Blandford R. D., Rees M. J., 1980, *Nature*, 287, 307
 Bell E. F., McIntosh D. H., Katz N., Weinberg M. D., 2003, *ApJS*, 149, 289
 Bell E. F., Phleps S., Somerville R. S., Wolf C., Borch A., Meisenheimer K., 2006, *ApJ*, 652, 270
 Bellovary J., Volonteri M., Governato F., Shen S., Quinn T., Wadsley J., 2011, *ApJ*, 742, 13
 Berczik P., Merritt D., Spurzem R., Bischof H.-P., 2006, *ApJ*, 642, L21
 Bernardi M., Shankar F., Hyde J. B., Mei S., Marulli F., Sheth R. K., 2010, *MNRAS*, 404, 2087
 Bernardi M., Meert A., Sheth R. K., Vikram V., Huertas-Company M., Mei S., Shankar F., 2013, *MNRAS*, 436, 697
 Berti E., Cardoso V., Gonzalez J. A., Sperhake U., Hannam M., Husa S., Brüggemann B., 2007, *Phys. Rev. D*, 76, 064034
 Berti E., Kesden M., Sperhake U., 2012, *Phys. Rev. D*, 85, 124049
 Bertin G., 2000, *Dynamics of Galaxies*. Cambridge Univ. Press, Cambridge
 Best P. N., von der Linden A., Kauffmann G., Heckman T. M., Kaiser C. R., 2007, *MNRAS*, 379, 894
 Binney J., 1980, *MNRAS*, 190, 873
 Binney J., Tremaine S., 1987, *Galactic Dynamics*. Princeton Univ. Press, Princeton, NJ
 Blecha L., Cox T. J., Loeb A., Hernquist L., 2011, *MNRAS*, 412, 2154
 Bogdanović T., Reynolds C. S., Miller M. C., 2007, *ApJ*, 661, L147
 Brenneman L., 2013, *Measuring the Angular Momentum of Supermassive Black Holes*. Springer-Verlag, New York
 Bryan G. L., Norman M. L., 1998, *ApJ*, 495, 80
 Bundy K., Fukugita M., Ellis R. S., Targett T. A., Belli S., Kodama T., 2009, *ApJ*, 697, 1369
 Buonanno A., Kidder L. E., Lehner L., 2008, *Phys. Rev. D*, 77, 026004
 Burke C., Collins C. A., 2013, *MNRAS*, 434, 2856
 Campanelli M., Lousto C. O., Marronetti P., Zlochower Y., 2006, *Phys. Rev. Lett.*, 96, 111101
 Campanelli M., Lousto C., Zlochower Y., Merritt D., 2007, *ApJ*, 659, L5
 Carollo C. M., Franx M., Illingworth G. D., Forbes D. A., 1997, *ApJ*, 481, 710
 Carrasco E. R. et al., 2010, *ApJ*, 715, L160
 Catinella B. et al., 2010, *MNRAS*, 403, 683
 Chandrasekhar S., 1943, *ApJ*, 97, 255
 Civano F. et al., 2010, *ApJ*, 717, 209
 Civano F. et al., 2012, *ApJ*, 752, 49
 De Lucia G., Blaizot J., 2007, *MNRAS*, 375, 2
 de Ravel L. et al., 2009, *A&A*, 498, 379
 Devecchi B., Rasia E., Dotti M., Volonteri M., Colpi M., 2009, *MNRAS*, 394, 633
 Do T. et al., 2014, *AJ*, 147, 93
 Dotti M., Colpi M., Haardt F., Mayer L., 2007, *MNRAS*, 379, 956
 Dotti M., Ruzsokowski M., Paredi L., Colpi M., Volonteri M., Haardt F., 2009, *MNRAS*, 396, 1640
 Dotti M., Volonteri M., Perego A., Colpi M., Ruzsokowski M., Haardt F., 2010, *MNRAS*, 402, 682
 Escala A., Larson R. B., Coppi P. S., Mardones D., 2004, *ApJ*, 607, 765
 Escala A., Larson R. B., Coppi P. S., Mardones D., 2005, *ApJ*, 630, 152
 Fanidakis N., Baugh C. M., Benson A. J., Bower R. G., Cole S., Done C., Frenk C. S., 2011, *MNRAS*, 410, 53
 Gerosa D., Kesden M., Berti E., O’Shaughnessy R., Sperhake U., 2013, *Phys. Rev. D*, 87, 104028

- Gerosa D., O’Shaughnessy R., Kesden M., Berti E., Sperhake U., 2014, preprint ([arXiv:e-prints](https://arxiv.org/abs/1408.0001))
- González J. A., Sperhake U., Brüggemann B., Hannam M., Husa S., 2007a, *Phys. Rev. Lett.*, 98, 091101
- González J. A., Hannam M., Sperhake U., Brüggemann B., Husa S., 2007b, *Phys. Rev. Lett.*, 98, 231101
- Gualandris A., Merritt D., 2008, *ApJ*, 678, 780
- Guo Q. et al., 2011, *MNRAS*, 413, 101
- Heckman T. M., Kauffmann G., Brinchmann J., Charlot S., Tremonti C., White S. D. M., 2004, *ApJ*, 613, 109
- Hernquist L., 1990, *ApJ*, 356, 359
- Hlavacek-Larrondo J., Fabian A. C., Edge A. C., Ebeling H., Allen S. W., Sanders J. S., Taylor G. B., 2013, *MNRAS*, 431, 1638
- Hoffman L., Loeb A., 2007, *MNRAS*, 377, 957
- Hopkins P. F., Richards G. T., Hernquist L., 2007, *ApJ*, 654, 731
- Hopkins P. F. et al., 2010, *ApJ*, 724, 915
- Hunter J. D., 2007, *Comput. Sci. Eng.*, 9, 90
- Kesden M., 2008, *Phys. Rev. D*, 78, 084030
- Kesden M., Sperhake U., Berti E., 2010a, *Phys. Rev. D*, 81, 084054
- Kesden M., Sperhake U., Berti E., 2010b, *ApJ*, 715, 1006
- Khan F. M., Just A., Merritt D., 2011, *ApJ*, 732, 89
- Khan F. M., Preto M., Berczik P., Berentzen I., Just A., Spurzem R., 2012, *ApJ*, 749, 147
- Khandai N., Di Matteo T., Croft R., Wilkins S. M., Feng Y., Tucker E., DeGraf C., Liu M.-S., 2014, preprint ([arXiv:e-prints](https://arxiv.org/abs/1408.0001))
- King A. R., Pringle J. E., 2006, *MNRAS*, 373, L90
- Kitzbichler M. G., White S. D. M., 2008, *MNRAS*, 391, 1489
- Klypin A. A., Trujillo-Gomez S., Primack J., 2011, *ApJ*, 740, 102
- Komossa S., 2012, *Adv. Astron.*, 2012, 364973
- Komossa S., Merritt D., 2008, *ApJ*, 683, L21
- Kormendy J., Ho L. C., 2013, *ARA&A*, 51, 511
- Koss M. et al., 2014, *MNRAS*, 445, 515
- Lacey C., Cole S., 1993, *MNRAS*, 262, 627
- Lackner C. N., Cen R., Ostriker J. P., Joung M. R., 2012, *MNRAS*, 425, 641
- Laporte C. F. P., White S. D. M., Naab T., Gao L., 2013, *MNRAS*, 435, 901
- Lauer T. R. et al., 2007, *ApJ*, 662, 808
- Li S., Liu F. K., Berczik P., Chen X., Spurzem R., 2012, *ApJ*, 748, 65
- Lidman C. et al., 2012, *MNRAS*, 427, 550
- Lidman C. et al., 2013, *MNRAS*, 433, 825
- Liu F. S., Mao S., Deng Z. G., Xia X. Y., Wen Z. L., 2009, *MNRAS*, 396, 2003
- Lodato G., Gerosa D., 2013, *MNRAS*, 429, L30
- Lodato G., Nayakshin S., King A. R., Pringle J. E., 2009, *MNRAS*, 398, 1392
- López-Sanjuan C. et al., 2011, *A&A*, 530, A20
- López-Sanjuan C. et al., 2012, *A&A*, 548, A7
- Lotz J. M., Jonsson P., Cox T. J., Croton D., Primack J. R., Somerville R. S., Stewart K., 2011, *ApJ*, 742, 103
- Lousto C. O., Zlochower Y., 2008, *Phys. Rev. D*, 77, 044028
- Lousto C. O., Zlochower Y., 2011, *Phys. Rev. Lett.*, 107, 231102
- Lousto C. O., Zlochower Y., 2013, *Phys. Rev. D*, 87, 084027
- Lousto C. O., Campanelli M., Zlochower Y., Nakano H., 2010, *Class. Quantum Gravity*, 27, 114006
- Lousto C. O., Zlochower Y., Dotti M., Volonteri M., 2012, *Phys. Rev. D*, 85, 084015
- Ludlow A. D., Navarro J. F., Angulo R. E., Boylan-Kolchin M., Springel V., Frenk C., White S. D. M., 2014, *MNRAS*, 441, 378
- Lynden-Bell D., 1967, *MNRAS*, 136, 101
- Macciò A. V., Dutton A. A., van den Bosch F. C., 2008, *MNRAS*, 391, 1940
- McConnell N. J., Ma C.-P., 2013, *ApJ*, 764, 184
- McConnell N. J., Ma C.-P., Murphy J. D., Gebhardt K., Lauer T. R., Graham J. R., Wright S. A., Richstone D. O., 2012, *ApJ*, 756, 179
- Malbon R. K., Baugh C. M., Frenk C. S., Lacey C. G., 2007, *MNRAS*, 382, 1394
- Merritt D., 2006, *ApJ*, 648, 976
- Merritt D., Poon M. Y., 2004, *ApJ*, 606, 788
- Merritt D., Milosavljević M., Favata M., Hughes S. A., Holz D. E., 2004, *ApJ*, 607, L9
- Merritt D., Schnittman J. D., Komossa S., 2009, *ApJ*, 699, 1690
- Miller M. C., Krolik J. H., 2013, *ApJ*, 774, 43
- Miller B., Gallo E., Treu T., Woo J.-H., 2012, *ApJ*, 747, 57
- Milosavljević M., Merritt D., 2003, in Centrella J. M., ed., *AIP Conf. Proc.* Vol. 686, *The Astrophysics of Gravitational Wave Sources*. Am. Inst. Phys. New York, p. 201
- Navarro J. F., Frenk C. S., White S. D. M., 1996, *ApJ*, 462, 563
- Navarro J. F., Frenk C. S., White S. D. M., 1997, *ApJ*, 490, 493
- Neto A. F. et al., 2007, *MNRAS*, 381, 1450
- Netzer H., Trakhtenbrot B., 2014, *MNRAS*, 438, 672
- Oser L., Ostriker J. P., Naab T., Johansson P. H., Burkert A., 2010, *ApJ*, 725, 2312
- Peacock J. A., 2003, preprint ([arXiv:e-prints](https://arxiv.org/abs/0309008))
- Peebles P. J. E., 1980, *The Large-Scale Structure of the Universe*. Princeton Univ. Press, Princeton, NJ
- Peebles P. J. E., 1993, *Principles of Physical Cosmology*. Princeton University Press, Princeton, NJ
- Perego A., Dotti M., Colpi M., Volonteri M., 2009, *MNRAS*, 399, 2249
- Posti L., Nipoti C., Stiavelli M., Ciotti L., 2014, *MNRAS*, 440, 610
- Postman M. et al., 2012, *ApJ*, 756, 159
- Preto M., Berentzen I., Berczik P., Spurzem R., 2011, *ApJ*, 732, L26
- Pretorius F., 2005, *Phys. Rev. Lett.*, 95, 121101
- Reynolds C. S., 2013, *Space Sci. Rev.*, 183, 277
- Rezzolla L., Barausse E., Dorband E. N., Pollney D., Reisswig C., Seiler J., Husa S., 2008, *Phys. Rev. D*, 78, 044002
- Robaina A. R., Bell E. F., van der Wel A., Somerville R. S., Skelton R. E., McIntosh D. H., Meisenheimer K., Wolf C., 2010, *ApJ*, 719, 844
- Russell H. R., McNamara B. R., Edge A. C., Hogan M. T., Main R. A., Vantyghem A. N., 2013, *MNRAS*, 432, 530
- Schnittman J. D., 2004, *Phys. Rev. D*, 70, 124020
- Schnittman J. D., 2007, *ApJ*, 667, L133
- Schnittman J. D., Buonanno A., 2007, *ApJ*, 662, L63
- Sesana A., 2010, *ApJ*, 719, 851
- Sesana A., 2013, *MNRAS*, 433, L1
- Sesana A., Barausse E., Dotti M., Rossi E. M., 2014, *ApJ*, 794, 104
- Shankar F., Croce M., Miralda-Escudé J., Fosalba P., Weinberg D. H., 2010, *ApJ*, 718, 231
- Shields G. A., Bonning E. W., 2013, *ApJ*, 772, L5
- Sonnenfeld A., Nipoti C., Treu T., 2014, *ApJ*, 786, 89
- Stott J. P. et al., 2012, *MNRAS*, 422, 2213
- Terzić B., Graham A. W., 2005, *MNRAS*, 362, 197
- Thorne K. S., 1974, *ApJ*, 191, 507
- Tichy W., Marronetti P., 2008, *Phys. Rev. D*, 78, 081501
- Tremaine S., Richstone D. O., Byun Y.-I., Dressler A., Faber S. M., Grillmair C., Kormendy J., Lauer T. R., 1994, *AJ*, 107, 634
- Trujillo I., Ferreras I., de La Rosa I. G., 2011, *MNRAS*, 415, 3903
- van den Bosch R. C. E., Gebhardt K., Gültekin K., van de Ven G., van der Wel A., Walsh J. L., 2012, *Nature*, 491, 729
- van der Marel R. P., Magorrian J., Carlberg R. G., Yee H. K. C., Ellingson E., 2000, *AJ*, 119, 2038
- Vasiliev E., Antonini F., Merritt D., 2014, *ApJ*, 785, 163
- Vicari A., Capuzzo-Dolcetta R., Merritt D., 2007, *ApJ*, 662, 797
- Volonteri M., Haardt F., Madau P., 2003, *ApJ*, 582, 559
- Volonteri M., Haardt F., Gültekin K., 2008, *MNRAS*, 384, 1387
- Volonteri M., Gültekin K., Dotti M., 2010, *MNRAS*, 404, 2143
- Wang J.-M. et al., 2009, *ApJ*, 697, L141
- Weinzirl T. et al., 2014, *MNRAS*, 441, 3083
- White S. D. M., Rees M. J., 1978, *MNRAS*, 183, 341
- Xu C. K., Zhao Y., Scoville N., Capak P., Drory N., Gao Y., 2012, *ApJ*, 747, 85

This paper has been typeset from a \LaTeX file prepared by the author.